Available online at www.sciencedirect.com
ScienceDirect
Geochimica et Cosmochimica Acta 75 (2011) 2828–2847
Geochimica et Cosmochimica Acta
www.elsevier.com/locate/gca

The effects of non-metabolizing bacterial cells on the precipitation of U, Pb and Ca phosphates

Sarrah Dunham-Cheatham [a,*], Xue Rui [b], Bruce Bunker [b], Nicolas Menguy [c], Roland Hellmann [d], Jeremy Fein [a]

[a] Department of Civil Engineering and Geological Sciences, University of Notre Dame, Notre Dame, IN 46556, USA
[b] Department of Physics, University of Notre Dame, Notre Dame, IN 46556, USA
[c] IMPMC-CNRS, UMR 7590, IPG Paris, Université de Paris 6 et 7, 140 rue de Lourmel, 75015 Paris, France
[d] Environmental Geochemistry Group, LGIT, CNRS, OSUG, Université J. Fourier, 38041 Grenoble Cedex 9, France

Received 20 September 2010; accepted in revised form 20 February 2011; available online 25 February 2011

Abstract

In this study, we test the potential for passive cell wall biomineralization by determining the effects of non-metabolizing bacteria on the precipitation of uranyl, lead, and calcium phosphates from a range of over-saturated conditions. Experiments were performed using Gram-positive *Bacillus subtilis* and Gram-negative *Shewanella oneidensis* MR-1. After equilibration, the aqueous phases were sampled and the remaining metal and P concentrations were analyzed using inductively coupled plasma-optical emission spectroscopy (ICP-OES); the solid phases were collected and analyzed using X-ray diffractometry (XRD), transmission electron microscopy (TEM), and X-ray absorption spectroscopy (XAS).

At the lower degrees of over-saturation studied, bacterial cells exerted no discernable effect on the mode of precipitation of the metal phosphates, with homogeneous precipitation occurring exclusively. However, at higher saturation states in the U system, we observed heterogeneous mineralization and extensive nucleation of hydrogen uranyl phosphate (HUP) mineralization throughout the fabric of the bacterial cell walls. This mineral nucleation effect was observed in both *B. subtilis* and *S. oneidensis* cells. In both cases, the biogenic mineral precipitates formed under the higher saturation state conditions were significantly smaller than those that formed in the abiotic controls.

The cell wall nucleation effects that occurred in some of the U systems were not observed under any of the saturation state conditions studied in the Pb or Ca systems. The presence of *B. subtilis* significantly decreased the extent of precipitation in the U system, but had little effect in the Pb and Ca systems. At least part of this effect is due to higher solubility of the nanoscale HUP precipitate relative to macroscopic HUP. This study documents several effects of non-metabolizing bacterial cells on the nature and extent of metal phosphate precipitation. Each of these effects likely contributes to higher metal mobilities in geologic media, but the effects are not universal, and occur only with some elements and only under a subset of the conditions studied.

1. INTRODUCTION

Mineral precipitation reactions affect the mobility and distribution of mass in a wide range of geochemical systems. Bacteria are ubiquitous in near-surface environments, and can control precipitation reactions in these systems through a number of biomineralization mechanisms. Two general classifications of biomineralization reactions have been described (Lowentam, 1981; Bazylinski and Moskowitz, 1997): biologically-induced mineralization (BIM) and biologically-controlled mineralization (BCM), both of which are driven by bacterial metabolic processes. In BIM, precipitation is not directly controlled by the

* Corresponding author. Tel.: +1 574 631 4534; fax: +1 574 631 9236.
E-mail address: sdunhamc@nd.edu (S. Dunham-Cheatham).

0016-7037/$ - see front matter © 2011 Elsevier Ltd. All rights reserved.
doi:10.1016/j.gca.2011.02.030

organism, but occurs in response to interactions between elements in bulk solution and metabolic exudates from the organism. For example, sulfate-reducing bacteria produce sulfide, which can react with aqueous Zn when released from the cell to precipitate extracellular sphalerite (ZnS) (Labrenz et al., 2000). In BCM, organisms expend energy to exert a direct control on precipitation, and the biominerals are used for a specific function and are typically located within a cell. For example, magnetotactic bacteria promote the internal formation of magnetite crystals for use as a navigational aide (Lefevre et al., 2009; Yu-Zhang et al., 2009).

There has been considerable speculation that a third type of biomineralization reaction, non-metabolic passive cell wall nucleation of minerals, occurs and that this process, integrated over time for the bacterial biomass in soils and surface water systems, represents a significant vector for transformation of aqueous ions to clay minerals and other inorganic and organic phases (e.g., Urrutia and Beveridge, 1994; Schultze-Lam et al., 1996). Both field (Ferris et al., 1987; Konhauser et al., 1993; Bonny and Jones, 2003; Fortin and Langley, 2005; Demergasso et al., 2007) and laboratory (Macaskie et al., 2000; Warren et al., 2001; Rivadeneyra et al., 2006) studies have examined mineral formation in super-saturated systems and have found a close spatial association between bacterial cells and a range of extracellular precipitated mineral phases. Despite the increasing number of studies to claim the importance of passive cell wall biomineralization (Lowenstam and Weiner, 1989; Châtellier et al., 2001; Ben Chekroun et al., 2004; Beazley et al., 2007; Dupraz et al., 2009), the nature of the evidence to date is equivocal. A range of studies have documented associations between bacterial cells and mineral precipitates (Konhauser, 1997, 1998; Arp et al., 1998; Douglas and Beveridge, 1998; Warren et al., 2001; Perez-Gonzalez et al., 2010), but a spatial association in and of itself does not prove a role of the cell wall in the precipitation reaction. Spatial associations between cells and precipitates that form away from the cells can be promoted through electrostatic attraction between cells and precipitates (Ams et al., 2004). Although passive binding of aqueous cations to anionic sites located within bacterial cell walls can affect the speciation and distribution of metals in bacteria-bearing systems (Beveridge and Murray, 1976; Fein et al., 1997; Kulczycki et al., 2002; Deo et al., 2010; Li and Wong, 2010), no study has demonstrated that this process affects mineral precipitation or that cell wall nucleation of precipitates can occur.

In addition to possible cell wall influences on precipitation, bacteria may influence mineral precipitation by exuding a range of organic molecules. For example, organic molecules exuded by biofilms widely affect the precipitation of calcite, influencing not only the growth kinetics, but the morphology as well (Mann et al., 1990; Archibald et al., 1996; McGrath, 2001; Meldrum and Hyde, 2001; Braissant et al., 2003; Hammes et al., 2003; Tong et al., 2004; Bosak and Newman, 2005; Dupraz et al., 2009), likely through incorporation effects (Lowenstam and Weiner, 1989). Studies have also shown that various organic molecules widely affect the structure and morphology of a range of minerals, including numerous iron oxides (Châtellier et al., 2001, 2004; Larese-Casanova et al., 2010; Perez-Gonzalez et al., 2010), uranyl phosphate (Macaskie et al., 2000), and silica (Williams, 1984).

In this study, we probed the role of non-metabolizing bacteria in the formation of metal phosphate minerals from over-saturated solutions. We selected U, Pb, and Ca in order to investigate metals that exhibit a broad range of binding affinities with phosphorus. In general, authigenic precipitation of minerals from saturated solutions in bacteria-rich settings is an important geochemical process in a number of natural and engineered geological systems, so it is crucial to understand bacterial effects on the precipitation reactions in order to model mass transport in these systems. For example, the exposure of Fe(II)-bearing anaerobic groundwaters to oxidizing bacteria-bearing conditions leads to Fe(III)-oxide precipitation and coating of mineral grains which is ubiquitous in subsurface environments (Schwertmann et al., 1985; Sullivan and Koppi, 1998). Phosphate systems are of particular interest due to the importance of P cycles and the low solubilities of many metal–phosphate phases. Reduction of Fe(III)-oxides by iron-reducing bacteria releases Fe(II) to solution and can lead to the precipitation of vivianite ($Fe_3(PO_4)_2{\cdot}8H_2O$), which is a major sink for Fe and for heavy metals in fresh water sedimentary systems (Taylor and Boult, 2007); anthropogenic contamination of groundwater and soil systems can lead to precipitation (or co-precipitation) of heavy metals as oxides and phosphate phases in these systems (e.g., Kirpichtchikova et al., 2006; Manceau et al., 2007; Terzano et al., 2007); and remediation strategies such as phosphate amendments rely on precipitation reactions in bacteria-bearing systems to reduce concentrations of dissolved metals in systems, such as those contaminated with dissolved U (e.g., Beazley et al., 2007; Martinez et al., 2007; Wellman et al., 2007; Ndiba et al., 2008) or by acid mine drainage (e.g., Schultze-Lam et al., 1996). The common denominator between all of these systems is the precipitation of phosphate and other mineral phases in environments that can be rich in non-metabolizing bacterial cells and/or bacterial exudates. Though most natural systems may not attain the degrees of supersaturation investigated in this study, some may, including mid-ocean ridge hydrothermal systems (Dekov et al., 2010), and groundwater mixing zones where ferrous iron oxidizes and precipitates as ferric oxide coatings (James and Ferris, 2004).

The objective of this study was to determine if, and under what conditions, the presence of non-metabolizing bacteria or bacterial exudates can influence precipitation reactions. Our experimental results can be used, therefore, to determine if the mobilities of the precipitating elements are likely to be markedly different than they would be if the precipitation occurred without bacteria present.

2. METHODS

2.1. General approach

We measured the nature and extent of metal phosphate precipitation as a function of aqueous saturation state in

systems that contained suspensions of non-metabolizing cells of either *Bacillus subtilis* or *Shewanella oneidensis*, comparing the results to those of abiotic controls. In the experiments, we created a range of over-saturated solutions by adding various concentrations of P in the form of Na_2HPO_4 to solutions containing dissolved U, Pb, or Ca in 0.1 M $NaClO_4$ in which washed, non-metabolizing bacterial cells were suspended. We sampled the aqueous phase and analyzed for total remaining metal and P in solution using ICP-OES. In addition, we characterized the solid phase of each system using TEM, XRD, and XAS.

2.2. Experimental methods

2.2.1. Bacterial preparation

Bacillus subtilis and *S. oneidensis* cells were grown aerobically in 5 mL of trypticase soy broth medium with 5% yeast extract for 24 h at 32 °C. The cells were then transferred to 1 L of trypticase soy broth medium with 5% yeast extract and incubated at 32 °C for another 24 h. The cells were then collected via centrifugation at 8100*g* for 5 min. The resulting pellet was washed five times with 0.1 M $NaClO_4$ (following a procedure described in more detail by Borrok et al., 2007), and pelleted after each wash using the centrifugation method described above. After five washes, the pellet was centrifuged for 1 h at 8100*g* to remove all excess liquid and to obtain a wet biomass value.

2.2.2. Kinetics experiments

Kinetics experiments were performed to determine the time required for the metal and P concentrations in the experiments to reach steady state. Precipitation experiments were prepared according to the method described below. Aqueous samples were extracted from each precipitation kinetics experiment at 0.25, 0.5, 1, 2, 4, 6, 18, 24, and 48 h. The samples were filtered through 0.2 μm PTFE syringe filters, acidified using trace metal grade 15.8 N HNO_3 at a sample:acid ratio of 5 mL:8 μL, and refrigerated pending ICP-OES analysis. Results (not shown) indicated that no change in metal or P concentration occurred after 2 h in the abiotic controls and the *B. subtilis* experiments, and after 3 h in the *S. oneidensis* experiments; all subsequent abiotic controls and *B. subtilis* experiments were allowed to react for 2 h, and subsequent *S. oneidensis* experiments were allowed to react for 3 h.

2.2.3. Batch precipitation experiments

To prepare the experiments, aqueous metal, P, and suspended bacteria parent solutions were mixed in different proportions to achieve the desired final concentrations. A $10^{-3.08}$ M U parent solution was prepared in a Teflon bottle by dissolving $UO_2(NO_3)_2$ in 0.1 M $NaClO_4$; a $10^{-2.30}$ M Ca parent solution was prepared in a Teflon bottle by dissolving $Ca(ClO_4)_2(H_2O)_4$ in 0.1 M $NaClO_4$; and a $10^{-3.02}$ M Pb parent solution was prepared in a Teflon bottle by diluting a commercially-supplied 1000 ppm aqueous Pb standard (in which the Pb is dissolved in 2% HNO_3) using 0.1 M $NaClO_4$; a $10^{-2.19}$ M P parent solution was prepared in a Teflon bottle by dissolving Na_2HPO_4 in 0.1 M $NaClO_4$. A 6.25 g (wet mass)/L bacterial parent solution was prepared by suspending a known mass of washed, non-metabolizing bacterial cells in 0.1 M $NaClO_4$.

Each experimental system was prepared by adding a weighed mass of bacterial parent suspension, followed by a weighed mass of the U, Ca, or Pb parent solution, to 0.1 M $NaClO_4$ in Teflon tubes to achieve the desired concentrations. The final parent solution to be added was the P one. In the U experiments, the initial U concentration was $10^{-4.20}$ M and the initial P concentrations ranged from $10^{-5.50}$ to $10^{-3.50}$ M. In the Pb experiments, the initial Pb concentration was $10^{-4.20}$ M and the initial P concentrations ranged from $10^{-5.50}$ to $10^{-3.50}$ M. The initial Ca concentration in all Ca experiments was $10^{-3.00}$ M and the initial P concentrations ranged from $10^{-5.00}$ to $10^{-2.00}$ M. The bacterial concentration for all biotic experiments ranged from 0.31 g wet biomass/L to 2.50 g wet biomass/L (the bacterial concentration for all results presented hereafter was 0.62 g wet biomass/L, unless otherwise noted), and the abiotic controls were conducted with identical metal and P concentrations to those used in the biotic experiments, but with no bacteria present. Cells were assumed to be non-metabolizing due to the lack of nutrients and electron donors in the suspensions; however, no direct confirmation of their metabolic state was performed. Inactivated cells could not be used as controls due to likely changes to cell wall chemistry and/or structure that accompany any passivation procedure.

After the P parent solution was added to each metal-bearing bacterial suspension, the pH of each experiment was adjusted immediately to the desired pH using 0.2 M HNO_3 and/or 0.2 M NaOH. The final pH values of the U, Pb, and Ca systems were 4.50 ± 0.10, 6.00 ± 0.10, and 8.00 ± 0.20, respectively. The pH of each experimental system was adjusted manually every 15 min throughout each experiment to maintain the desired pH, except for the last thirty minutes during which the experiments were undisturbed. In general, the pH drifted slightly toward circum-neutral values, but only minor adjustments, if any, were necessary after the first hour of each experiment. The suspensions were constantly agitated on an end-over-end rotator at 40 rpm for the duration of the experiment. After the prescribed equilibration time, all suspensions were centrifuged at 8100*g* for 5 min. The supernatant was filtered through 0.2 μm PTFE syringe filters, acidified using trace metal grade 15.8 N HNO_3 at a sample:acid ratio of 5 mL:8 μL, and refrigerated pending ICP-OES analyses. The solid phase was maintained at 4 °C pending XRD, TEM, and XAS analysis. All U and Pb experiments were conducted under atmospheric conditions, and all Ca experiments were conducted in a N_2/H_2 atmosphere in order to exclude atmospheric CO_2 and to prevent possible calcium carbonate precipitation. All experiments were performed in triplicate by conducting three independent experiments.

2.2.4. Precipitation experiments using bacterial exudate solution

A solution containing bacterial exudate molecules with no cells present was prepared in the following manner: *B. subtilis* cells were added to 0.1 M $NaClO_4$ to reach a

concentration of 0.62 g wet biomass/L. The pH of the suspension was adjusted to 4.50 ± 0.10 using small amounts 0.2 M HCl and/or 0.2 M NaOH. The pH was monitored every 15 min and adjustments were made for 2 h. The suspension was then centrifuged at 8100*g* for 10 min to remove all bacteria from solution. An aliquot of the supernatant was immediately collected, filtered through a 0.2 μm PTFE syringe filter, and acidified using 15.8 N HNO_3 at a sample:acid ratio of 5 mL:8 μL. This sample was analyzed with ICP-OES to determine the starting concentration of P in the exudate solution and with a total organic carbon (TOC) analyzer to determine the concentration of dissolved carbon in the solution. The resulting concentrations were $10^{-5.41\pm0.74}$ M P and 2.71 ± 0.17 ppm C. The remainder of the supernatant was then used in place of the 0.1 M $NaClO_4$ in an abiotic control precipitation experiment for the U system only. At the completion of the experiment, samples were collected and analyzed as described above.

2.2.5. Biogenic mineral isolation

As we describe below, the U experiments were the only ones to yield cell wall-nucleated biomineralization under some of the conditions studied. In order to measure the solubility of these precipitates in separate experiments, we isolated the particles from their cell wall framework using a procedure similar to the one described by Ulrich et al. (2008). Biotic U precipitation experiments were prepared according to the above method using *B. subtilis* cells. After the prescribed equilibration time, the biomass was centrifuged for 5 min at 8100*g*, and the supernatant was decanted. The bacteria/mineral pellet was re-suspended in a 20% bleach solution, diluted with 18 MΩ ultrapure water, and placed on a rotating table at 32 °C overnight. The suspension was centrifuged for 10 min at 8100*g* and decanted. The pellet was then rinsed three times with 18 MΩ ultrapure water, until the pH of the wash supernatant was circum-neutral, centrifuging for 10 min at 8100*g* and decanting between each rinse. The pellet was suspended in 10 mL of 18 MΩ ultrapure water, transferred into a 60 mL separatory funnel, and 50 mL of hexane was added to separate the organic debris from the minerals. The funnel was capped and shaken vigorously for 3 min, then left undisturbed overnight. The water portion was collected, centrifuged for 10 min at 8100*g*, and the supernatant was decanted. The pellet was rinsed once with 18 MΩ ultrapure water, then centrifuged for 10 min at 8100*g* and decanted. The bleach/hexane process was repeated until no bacterial remnants were present in the collected sample as determined by optical microscopy. Once the biogenic minerals were isolated, the pellet was washed a final time with 18 MΩ ultrapure water, centrifuged for 10 min at 8100*g*, the supernatant was decanted, and the particles were allowed to air dry. XRD analysis of the biogenic minerals suggested that the minerals were unaffected by the bleach/hexane treatment, and that they had the same crystal structure as the precipitates that formed in the parallel abiotic controls (Fig. EA1). Scanning electron microscopy (SEM) analysis showed that the minerals were needle-like with a length ranging from 10 to 30 nm.

2.2.6. Solubility experiments

Separate solubility experiments were performed using the isolated and washed biogenic HUP particles. A known mass of the dry mineral powder was transferred to a Teflon tube and 18 MΩ ultrapure water was added to reach a concentration of 3 g/L. Small aliquots of 0.2 M HNO_3 or 0.2 M NaOH were added to adjust the pH of the solution to 4.20 ± 0.10. The pH of the solution was adjusted every hour in the first 24 h until the pH value remained within the desired range. A 2 mL sample was extracted after 24 h, and every 48 h after that for a total of 23 days. After extraction, samples were filtered immediately through 0.2 μm PTFE syringe filters, gravimetrically diluted with 18 MΩ ultrapure water, acidified using trace metal grade 15.8 N HNO_3 at a sample:acid ratio of 5 mL:8 μL, and refrigerated pending ICP-OES analysis of dissolved U and P concentrations.

2.3. Analytical methods

2.3.1. TEM

Using TEM, we examined the solid phase run products from both abiotic and biotic samples, and from a high and low saturation state for each metal system studied. For the U system, the P concentration conditions studied with TEM were $10^{-4.49}$ (sample U5), $10^{-3.89}$ (U8), $10^{-3.65}$ (U10), and $10^{-3.49}$ M (U11) (Table 1); for the Pb system, the P concentration conditions studied were $10^{-4.49}$ (Pb4), $10^{-3.79}$ (Pb6), $10^{-3.65}$ (Pb7), and $10^{-3.49}$ M (Pb8) (Table 2); for the Ca system, the P concentration conditions studied were $10^{-3.09}$ (Ca4), $10^{-2.49}$ (Ca7), and $10^{-2.01}$ M (Ca11) (Table 3). At the completion of each precipitation experiment, the pellet was suspended in a 2% gluteraldehyde fixative solution. The suspension was rotated end-over-end for 1 h, then centrifuged and decanted. The pellet was rinsed three times with 18 MΩ ultrapure water. The suspension was suspended in a 0.2% OsO_4 fixative solution and rotated end-over-end for 1 h, then centrifuged and decanted. The pellet was rinsed three times with 18 MΩ ultrapure water. The pellet was subjected to a series of ethanol solutions, starting at 50% ethanol and ending with 100% ethanol, to remove all water from the pellet. The dehydrated pellet was suspended in a series of Spurs resin solutions, starting with a 1:1 mixture of resin and 100% ethanol and ending with 100% resin, enabling infiltration of the bacteria by the resin. The infiltrated pellet was placed in the tip of a 1 mL BEEM capsule, and the capsules were filled with 100% resin and placed in a 70 °C oven for 24 h. The sample blocks were removed from the capsules, sectioned by ultramicrotomy to a 110 nm thickness, and mounted onto 200 mesh copper grids. Only the grids for the Pb and Ca systems were stained with uranyl acetate and lead citrate; the U system grids were not stained. TEM images were collected using a Hitachi H-600 TEM operated at 75 kV acceleration voltage, as well as a JEOL 2100F TEM operated at 200 kV using various modes: bright field (BF), dark field (DF), and scanning TEM (STEM). Chemical maps were determined by an electron dispersive X-ray (EDX) detector using the *K* line for P and the *M* line for U using the JEOL 2100F TEM.

2.3.2. XRD

Some of the solids from the abiotic control experiments and from the biotic experiments were selected for detailed characterization by XRD. These solids were ground into a fine powder using acetone and an alumina mortar and pestle. The slurry was transferred onto a zero-background silica XRD slide and allowed to air dry. The slide was then measured at room temperature using a Scintag X-1 Powder XRD with a copper radiation source. Data were collected every half-degree from 5 to 60 degrees.

2.3.3. Synchrotron experiments

The solid run products from four biotic experiments and from the corresponding four abiotic controls in the U system were prepared for XAS analysis to characterize the crystallinity and structure of the precipitates. The concentrations of P in these four experiments were $10^{-4.49}$ (sample U5), $10^{-3.89}$ (sample U8), $10^{-3.65}$ (sample U10), and $10^{-3.49}$ (sample U11) M (Table 1). Resulting bacteria/mineral pellets were immediately packaged on ice for overnight shipment. X-ray absorption near edge structure (XANES) and extended X-ray absorption fine structure (EXAFS) at the U L_3-edge (17166) were collected at room temperature for all pellets. A silicon (1 1 1) crystal monochromator was used to select a single energy beam. A Rh-coated harmonic rejection mirror was used to further eliminate the high harmonic component in the beam. The incident ionization chamber was filled with 100% N_2 gas, and the transmission and reference ionization chambers were filled with 50% N_2 gas and 50% Ar gas, respectively. All of the spectra were collected in transmission mode as the fluorescence spectra suffered self-absorption problems due to the high concentration of uranyl phosphate mineral in the samples (Bunker, 2010).

Abiotic control samples were precipitated and air dried before processing. Samples were ground into fine powder using a corundum mortar and pestle, then mixed with graphite powder to reach relative homogeneity before being loaded into Plexiglas holders and sealed with Kapton film. At the energy of the U L_3-edge, the extra coverage of Kapton film did not affect the measurements. Biotic samples, present as a paste, were prepared for measurement by loading the paste into slotted Plexiglas holders, which were then covered with Kapton film. Prepared biotic samples were refrigerated until data collection. All measurements were conducted within 72 h of sample preparation.

For every sample, 10 XANES spectra were initially collected, each lasting less than a minute, in order to monitor for possible radiation damage to the sample. Due to the heterogeneity of the samples, EXAFS spectra were collected after the XANES measurements at 10 different spots, with two measurements at each spot. No radiation damage was observed in the spectra within the 1 min data acquisition period.

The data were processed using the UWXAFS package (Stern et al., 1995). The program Athena (Ravel and Newville, 2005) was used to remove the background using the AUTOBK algorithm (Newville et al., 1993) and to convert the data from k space into R space via Fourier transformation. The cutoff of background-*Rbkg* was set to 1.1 for all measurements. The program Artemis (Ravel and Newville, 2005) was used to fit the experimental EXAFS spectra. Well defined mineral structures were input into Atom (Ravel et al., 2001) and used to generate theoretical EXAFS paths in FEFF6 (Zabinsky et al., 1995). Shell-by-shell fitting was obtained using the program FEFFIT (Newville, 2001), and the statistical factors reduced-χ^2 and R-factor were used as criteria to optimize the fitting.

2.3.4. ICP-OES

ICP-OES element standards with the same ionic strength matrix as the experimental samples were prepared gravimetrically by diluting commercially-supplied 1000 ppm aqueous Ca, Pb, U, and P standards with 0.1 M $NaClO_4$. The concentrations of the U and Pb standards ranged from $10^{-6.70}$ to $10^{-4.10}$ M. The concentrations of the Ca standards ranged from $10^{-4.90}$ to $10^{-3.00}$ M, and the concentrations of the P standards ranged from $10^{-5.80}$ to $10^{-2.60}$ M. The standards were acidified following the same procedure as was applied to the samples. The standards and samples were analyzed with a Perkin Elmer 2000DV ICP-OES within 5 days of collection. U was analyzed at 424.167 nm, Pb was analyzed at 220.356 nm, Ca was analyzed at 227.546 nm, and P was analyzed at 214.914 nm. The set of standards was analyzed before, in between, and after the samples were analyzed to check for machine drift. Analytical uncertainty, as determined by repeat analyses of the standards, was ±2.75%.

2.3.5. TOC

TOC standards were prepared by gravimetrically diluting commercially-supplied 1000 ppm C aqueous standard using the same ionic strength buffer solution as the experimental samples. The standards were then acidified with 6 M HCl and immediately sealed with parafilm. The standards and samples were analyzed with a Shimadzu TOC – V/TNM within 24 h of collection.

2.4. Thermodynamic modeling

2.4.1. Saturation states calculations

To determine initial saturation state values for each of the experimental systems, activity quotients (Q) were calculated using a Newton–Raphson iteration technique to solve the non-linear system of mass balance and mass action

Table 1
Starting conditions for precipitation experiments (U system).

ID	Initial [U] (log M)	Initial [P] (log M)	Saturation index (log (Q/K))	XRD	TEM and XAS
U1	−4.20	−5.49	0.74		
U2	−4.20	−5.09	1.13		
U3	−4.20	−4.79	1.41		
U4	−4.20	−4.62	1.58		
U5	−4.20	−4.49	1.69	✓	✓
U6	−4.20	−4.19	1.94		
U7	−4.20	−4.01	2.07		
U8	−4.20	−3.89	2.14	✓	✓
U9	−4.20	−3.79	2.20		
U10	−4.20	−3.65	2.27	✓	✓
U11	−4.20	−3.49	2.32	✓	✓

Table 2
Starting conditions for precipitation experiments (Pb system).

ID	Initial [Pb] (log M)	Initial [P] (log M)	Saturation index (log (Q/K))	XRD	TEM
Pb1	−4.20	−5.79	4.29		
Pb2	−4.20	−5.19	4.91		
Pb3	−4.20	−4.71	5.77		
Pb4	−4.20	−4.49	6.20	✓	✓
Pb5	−4.20	−4.01	7.15		
Pb6	−4.20	−3.79	7.60	✓	✓
Pb7	−4.20	−3.65	7.89		✓
Pb8	−4.20	−3.49	8.19	✓	✓

Table 3
Starting conditions for precipitation experiments (Ca system).

ID	Initial [Ca] (log M)	Initial [P] (log M)	Saturation index (log (Q/K))	XRD	TEM
Ca1	−3.00	−4.49	2.31		
Ca2	−3.00	−3.79	5.25		
Ca3	−3.00	−3.49	5.26		
Ca4	−3.00	−3.09	6.36	✓	✓
Ca5	−3.00	−2.79	7.12		
Ca6	−3.00	−2.62	7.51		
Ca7	−3.00	−2.49	7.75	✓	✓
Ca8	−3.00	−2.31	8.04		
Ca9	−3.00	−2.19	8.20		
Ca10	−3.00	−2.09	8.29		
Ca11	−3.00	−2.01	8.34	✓	✓

equations listed in Tables EA1, EA2, and EA3. The starting molarities of each metal and P were used as mass balance constraints, and the resulting Q was calculated according to the following dissolution reactions for hydrogen uranyl phosphate, lead phosphate, and hydroxylapatite:

$$(UO_2)(HPO_4)3H_2O \leftrightarrow 3H_2O + UO_2^{2+} + HPO_4^{2-} \quad (1)$$

$$Pb_3(PO_4)_2(s) \leftrightarrow 3Pb^{2+} + 2PO_4^{3-} \quad (2)$$

$$Ca_5(PO_4)_3OH_{(s)} \leftrightarrow 5Ca^{2+} + 3PO_4^{3-} + OH^- \quad (3)$$

so that the Q value for each reaction corresponds to the following terms, respectively:

$$Q_U = a_{H_2O}^3 \cdot a_{UO2} \cdot a_{HPO_4} \quad (4)$$

$$Q_{Pb} = a_{Pb}^3 \cdot a_{PO_4}^2 \quad (5)$$

$$Q_{Ca} = a_{Ca}^5 \cdot a_{PO_4}^3 \cdot a_{OH} \quad (6)$$

Activity coefficients were calculated using an extended Debye–Hückel equation with A, B, and $\mathring{a}$ values of 0.5101, 0.3285, and 5.22, respectively (Helgeson et al., 1981). Saturation state values were then calculated by comparing the resulting Q values to the equilibrium constants, K, for the respective mineral, according to Eq. 7:

$$\text{Saturation Index} = \log(Q/K) \quad (7)$$

In the calculations, we assume water activities of unity, and the equilibrium constant values that were used for Reactions 1–3 were $10^{-13.17}$, $10^{-43.53}$, and $10^{-53.28}$, respectively (Martell and Smith, 2001; Gorman-Lewis et al., 2009; Zhu et al., 2009).

2.4.2. HUP solubility calculation

The solubility of the isolated biogenic HUP particles was calculated using a similar Newton–Raphson program to the one used to calculate saturation states to solve the non-linear set of mass action and mass balance equations corresponding to the reactions listed in Table EA1. The total dissolved P concentration for the calculation was fixed at the average P concentration from the biogenic HUP solubility experiments. The model was used to calculate the expected U concentration based on the solubility product for macroscopic HUP reported by Gorman-Lewis et al. (2009).

3. RESULTS AND DISCUSSION

3.1. Uranium system

3.1.1. TEM

Element maps (a representative example of which is shown in Fig. 1) of U and P distributions in the biotic *B. subtilis* samples indicate that while P is distributed throughout the cells, U is concentrated on the cell walls. These results suggest that the cells in these experiments did not actively incorporate U into the cytoplasm through metabolic processes, and that the U distribution in the biotic experiments is controlled by adsorption and/or precipitation reactions on or within the bacterial cell walls.

The TEM images of the samples taken from the lower saturation state conditions investigated (samples U5 and U8) suggest that precipitation of uranyl phosphates was homogeneous, occurring exclusively in solution, and that the cell walls did not appear to influence the mineralization reaction (Fig. 2A and B). The figures show some contact between the precipitate and the bacterial cells in these samples, but the images do not offer evidence that the cells were involved in the precipitation, and it is likely that the cell-mineral association is coincidental only. Fig. 2A and B also show no significant difference in the size of the mineral precipitate between the abiotic control and the biotic experiment, which is consistent with a lack of influence of the bacterial cells on the precipitation reaction at the lower saturation state conditions investigated.

TEM evidence, however, indicates that under the higher saturation state conditions investigated (sample U11), uranyl phosphate precipitation was heterogeneous, with nano-scale crystals appearing to nucleate within the three-dimensional macromolecules that comprise the bacterial cell walls (Fig. 2C and D). Under these conditions, there is a distinct difference in precipitate size between the abiotic control and the biotic experiment. The abiotic control (Fig. 2C) exhibits plate-like precipitates with edge lengths ranging from approximately 50 to 150 nm and thicknesses of approximately 10 nm. The lath-like precipitates observed in the abiotic controls represent cross-sections of the plate-like precipitates that are oriented perpendicular to the plane of the page. Close examination of the cell wall-controlled precipitation (Fig. 3) demonstrates that precipitation was uniformly distributed around each cell and that the crystals are all plate-like in morphology with edge lengths ranging from approximately 10 to 30 nm and a thickness of approximately 1 to 5 nm, with nucleation occurring throughout the

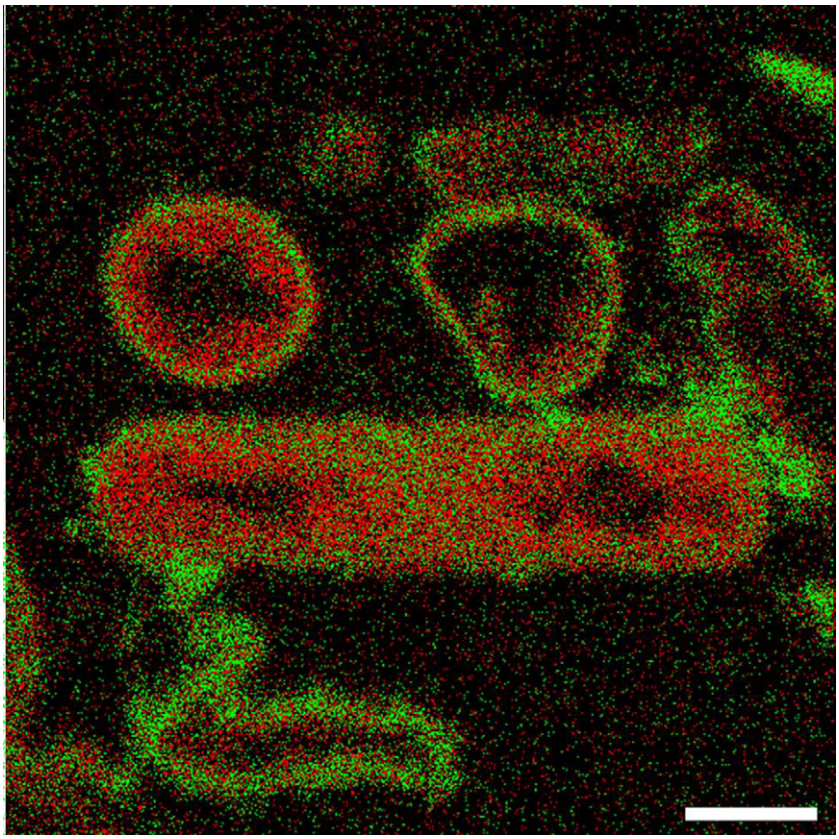

Fig. 1. Elemental map of biotic (*Bacillus subtilis*) U11 sample. P is shown in red, U is shown in green. The scale bar is 500 nm. (For interpretation of the references to colour in this figure legend, the reader is referred to the web version of this article.)

cell wall matrix and with crystals growing both into and out of the cell itself. The same cell wall nucleation phenomenon was observed in samples from the parallel systems that contained *S. oneidensis* MR-1 (Fig. 4); however, with the Gram-negative species, the nucleation appears to be restricted between the outer and plasma membranes, and the particles are oriented parallel to the cell membranes. This can be compared to the randomly oriented crystals that formed within the cell wall matrices of the Gram-positive *B. subtilis* species.

These images provide unequivocal evidence that bacterial cell walls can nucleate mineral formation. The particles visible within the bacterial cell walls depicted in Figs. 2D, 3, and 4 clearly nucleated in place, most likely nucleated on one or more types of cell wall functional groups. Surface controlled precipitation is thought to stem from adsorption onto surface binding sites (e.g., Farley et al., 1985; Warren and Ferris, 1998), and in the experiments in which cell wall nucleation was evident, precipitation likely begins with uranyl adsorption onto a cell wall binding site. The adsorbed uranyl forms a positively charged site, and in this way phosphate adsorption can alternate with uranyl adsorption at this site to form a bacterial cell wall precipitate.

3.1.2. SAED and XRD

Selected area electron diffraction (SAED) patterns of the abiotic run products tested indicated that the precipitated solids exhibit a high degree of crystallinity. SAED results for the biotic samples exhibit a diffuse ring pattern, with some evidence of weak and ephemeral diffraction patterns. This is evidence that the nanoparticles are crystalline, but because of their small size they rapidly become amorphous under the electron beam. Solid run products from abiotic controls and biotic experiments with starting P concentrations of $10^{-4.49}$, $10^{-3.89}$, $10^{-3.65}$, and $10^{-3.49}$ M, the same samples (U5, U8, U10, and U11) that were analyzed with TEM, were characterized using XRD to determine the crystallinity and identity of the precipitates. Each of the samples exhibits a number of peaks in common with the diffractogram for a reference sample of hydrogen uranyl phosphate ($UO_2HPO_4{\cdot}4H_2O$), or HUP, as well as some different peaks (Fig. 5). Each of the sample diffractograms exhibit peak shoulders at 2θ equal to 24.25 and 25.75 that correspond to characteristic peak angles in the reference pattern. Similarly, the reference pattern and all of the samples exhibit a peak at 2θ equal to 51.75. Additionally, all of the biotic experiments exhibit a peak at 2θ equal to 27.25, which corresponds with the peak at the same angle in the reference pattern. However, the peaks exhibited at 2θ equal to 22.7 are only present in the biotic U8 and U10 experiment diffractograms, and not exhibited in the reference pattern. These peaks are likely a result of minor, unidentified mineral phases only present in the biotic samples, or they may result from the HUP in the sample containing a differ-

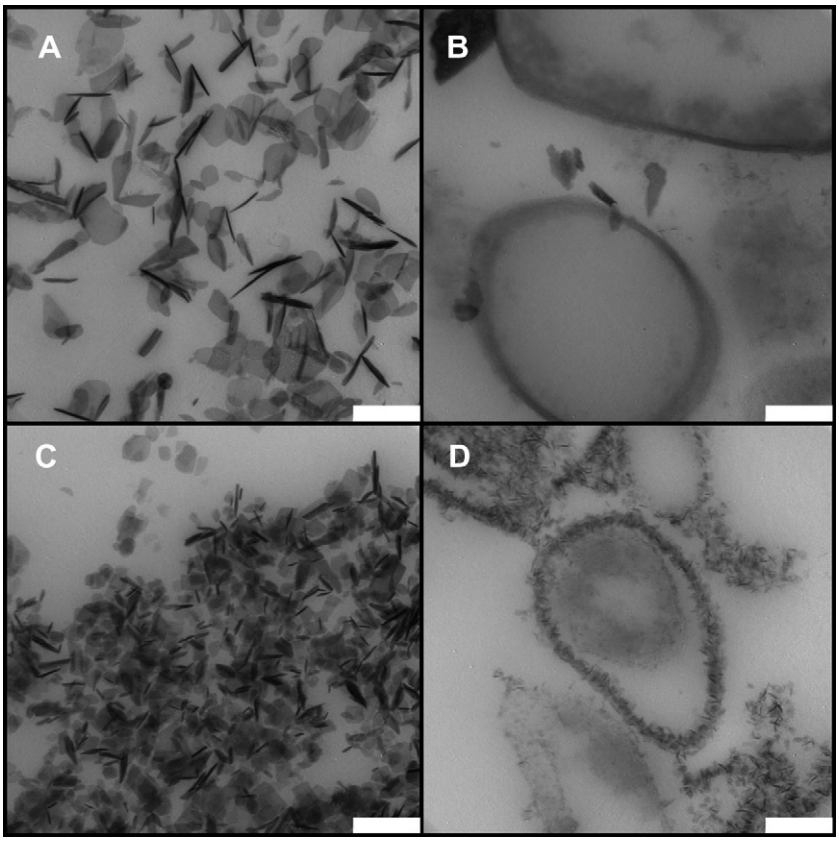

Fig. 2. TEM bright field images for U system: (A) Abiotic U5 control; (B) Biotic U5 experiment; (C) Abiotic U11 control; (D) Biotic U11 experiment. All scale bars are 200 nm. The bacteria in (B) and (D) is *B. subtilis*.

ent number of water molecules than the HUP XRD standard. Additionally, the peak at 2θ equal to 24.7 in the bacteria-only sample is present in diffractograms for each abiotic and biotic sample, but is not present in the diffractogram for the mineral reference sample. This peak likely results from a salt precipitate from the experimental solutions. Although there are variations in peak intensities in the diffractograms between the precipitates from the abiotic controls and the biotic experiments, and between precipitates from experiments with varying P concentrations, the peak positions and intensities in each diffractogram are consistent with the HUP reference pattern.

3.1.3. XAS

XANES spectra (Fig. EA2) indicate a U(VI) valence state for all of the samples, with no reduction of U to U(IV) observed. The edge position of the U(IV) spectrum is shifted approximately 4 eV towards lower energy relative to the U(VI) spectrum (Kelly et al., 2002), and this shift was not observed in any of our samples. The shoulder structure approximately 15 eV above the edge due to the multiple-scattering of the two axial oxygen atoms of the uranyl ion (Hennig et al., 2001) is a characteristic feature of the U(VI) valence state (Boyanov et al., 2007), and is present in the spectra of all of our samples. Both lines of evidence indicate that the vast majority of the uranium in our biotic and abiotic samples remained as U(VI) during the experiments, with no measureable reduction to U(IV).

EXAFS spectra at the U L_3-edge show that at low saturation state conditions (biotic sample U5), uranyl ions are present in the biotic sample dominantly as adsorbed species, bound to carboxyl and phosphoryl groups on the bacterial cell walls. The signal strength of the phosphorous peak (located at 3.0 Å) is weak compared to the HUP reference spectrum (Fig. 6), and in general, the biotic U5 sample exhibits a markedly different spectrum than does the HUP standard. The second oxygen peak is more distinguishable from the other samples, and the peak at approximately 3.0 Å is damped. At 2.2 Å, the biotic U5 spectrum does not dip as much as the HUP mineral spectrum, which corresponds to the contribution of a carbon atom. The fitting suggests a binding environment of two axial oxygen atoms at 1.75 Å, and two split equatorial oxygen shells: one at 2.19 Å with approximately 2.2 oxygen atoms, and the other at 2.34 Å with approximately 5.3 oxygen atoms. This split of the equatorial oxygen shells results from the uranyl ion binding to a phosphate group so that the symmetry of equatorial oxygen is perturbed. The average number of bound C atoms at 2.90 Å from the U atom is 1.1, and the average number of bound P atoms at a distance of 3.54 Å is 0.78. These results suggest that the uranyl ion in biotic sample U5 is bound to both carboxyl and phosphoryl sites, a result that is consistent with the findings of Kelly

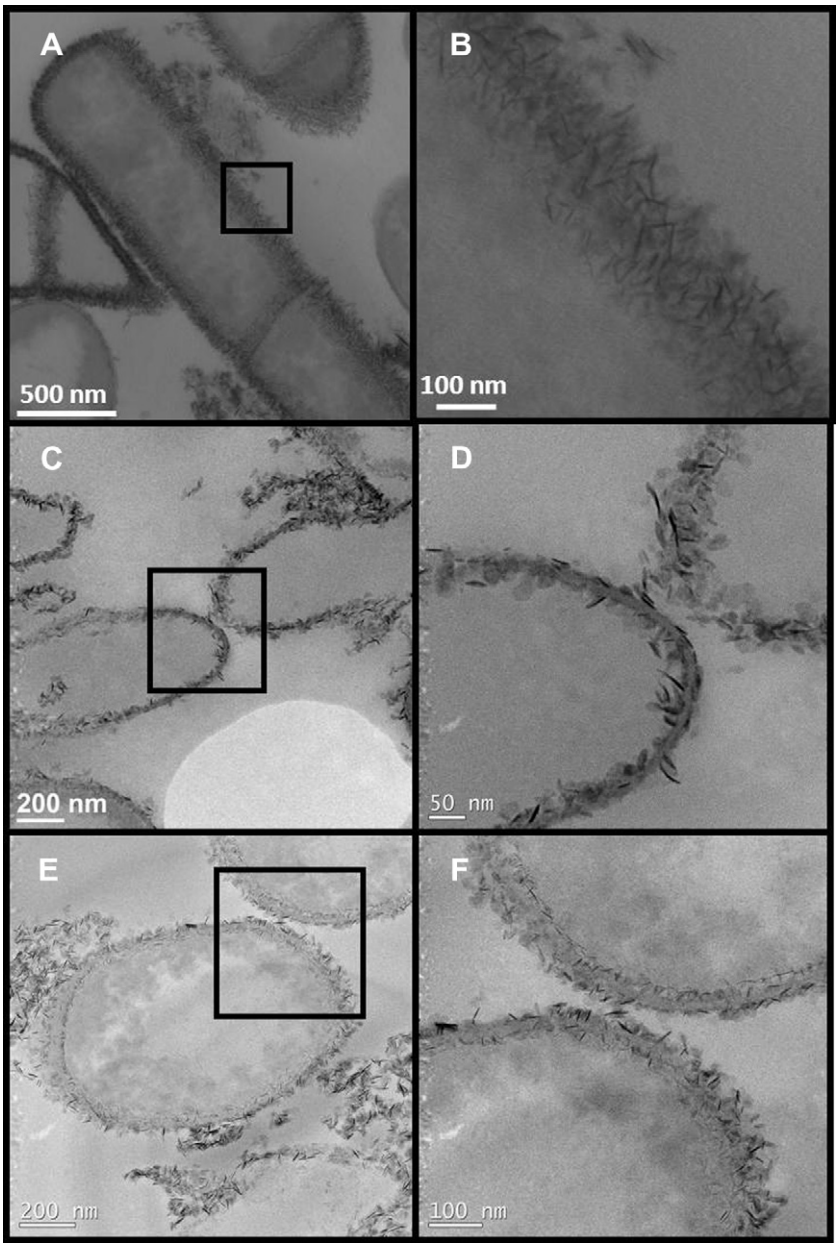

Fig. 3. TEM bright field images for U system: (A) Biotic U10 experiment; (B) close up of area located in the black box in image A to illustrate the texture of the biogenic U nanoparticulate precipitate; (C) Biotic U10 experiment; (D) close up of area located in the black box in image C; (E) Biotic U10 experiment; (F) close up of area located in the black box in image E. The bacteria in all micrographs is *B. subtilis*.

et al. (2002) who examined the adsorption of uranyl onto *B. subtilis* cells. The model fit of this EXAFS spectrum is shown in Fig. EA3.

Although adsorbed U is the only form of U detected by XAS in the biotic U5 sample, with increasing saturation state conditions, the EXAFS spectra indicate that U is present predominantly as solid phase HUP. Fig. 6 compares the EXAFS spectra from the abiotic and biotic samples with that of the HUP standard. All the abiotic samples and most of the biotic samples (except biotic U5) match the HUP mineral spectrum, exhibiting an axial oxygen peak at 1.4 Å, an equatorial oxygen peak at 1.8 Å, and a peak at 3.0 Å. (corresponding to phosphorus atoms). Slight differences exist between the spectra from the abiotic and the biotic samples, but these are likely due to experimental artifacts from the sample preparation procedure. Heterogeneous samples are well known to exhibit amplitude reduction, known as "thickness effects", in transmission measurements, and can also introduce background variations in the spectra. Because only small amounts of the abiotic precipitates were available for the experiment, the dried precipitates were ground and mixed with graphite powder before being mounted for measurement to obtain relatively homogenous samples. The EXAFS spectra were taken from

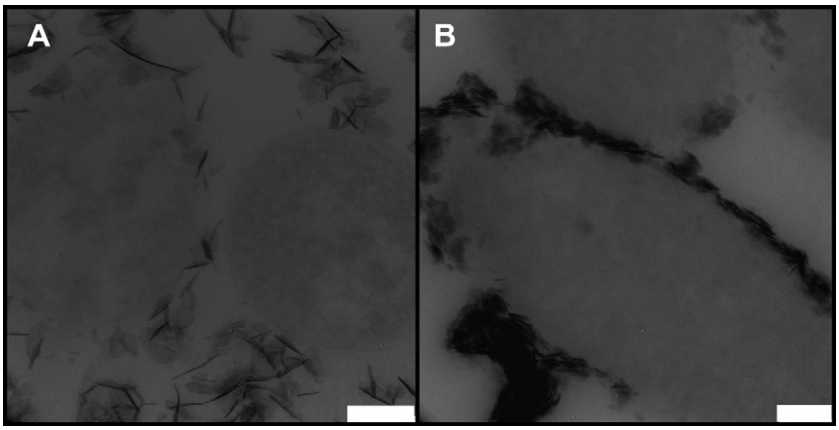

Fig. 4. TEM bright field image of uranyl phosphate biomineralization in biotic (A) U5 and (B) U11 samples, showing texture and prevalence of minerals within the *S. oneidensis* cell walls. The scale bars represent (A) 200 nm, and (B) 100 nm.

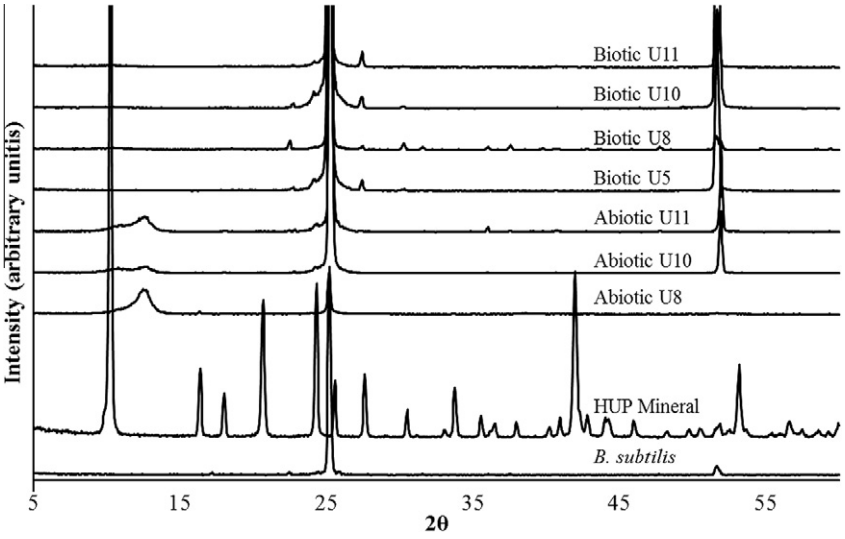

Fig. 5. XRD patterns from analysis of run products from U system experiments.

different spots of the sample, and the spots which exhibited obvious anomalous background were abandoned. Despite these efforts to eliminate the artifacts from heterogeneity, spectra from some samples still exhibited background anomalies. In addition to the background artifacts, the possibility of amorphous phases existing together within the mineral crystal cannot be ignored. In the amorphous phase, the disorder of the local structure around uranium would reduce the amplitudes of the oxygen peaks. The biotic samples, on the other hand, were more homogenous as a result of the biomass matrix. The differences in biotic samples were relatively small, except for the biotic U5 sample, which indicates U ions adsorbed to the bacterial cell wall rather than nanoparticle formation. Fluorescence measurements (data not shown here) of the samples in Fig. 6 are consistent with transmission measurements, which corroborates the validity of the measurements.

The k^3-weighted EXAFS spectra (Fig. EA2) show the suppressed oscillations around k∼10, which is a characteristic signature for HUP/autunite/chernikovite group minerals (Fuller et al., 2003). This feature is present in every sample (except biotic U5), which supports the conclusion that the dominating phase in the abiotic and biotic samples is the HUP mineral phase. With the exception of the biotic U5 sample, all of the spectra could be fit to the HUP structure (Morosin, 1978) with 2 axial oxygen atoms at 1.78 Å, approximately 4 equatorial oxygen atoms at 2.3 Å, and approximately 4 phosphorus atoms at 3.6 Å. The fitting to each spectrum is shown in Fig. EA3 (details of the fitting paths and parameters are available in Tables EA4 and EA5). Fittings show consistent distances between the axial and equatorial oxygen and uranium as well as the phosphorus and uranium atoms compared to the known HUP structure. The shell coordination numbers are also consistent, within uncertainty, with the HUP structure. Multiple scattering paths from the axial oxygen atoms and from the equatorial oxygen-phosphorous atoms were also included to improve the quality of the fit.

The XAS results indicate that bacteria do not affect the mineral that precipitates during our experiments, and that

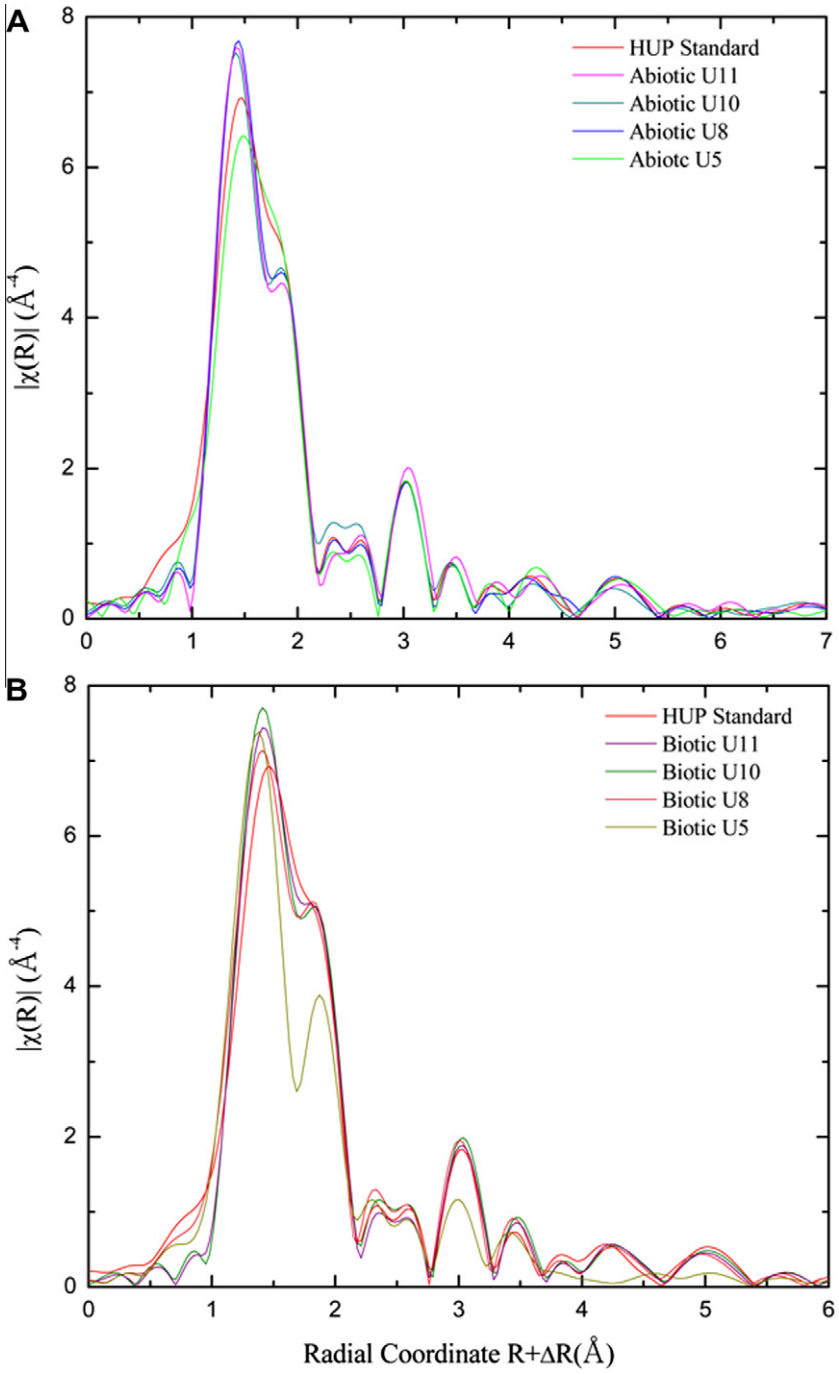

Fig. 6. (A) Magnitude of U L_3-edge EXAFS spectrum after Fourier transformation for the abiotic sample overlaid by the HUP standard. (B) Magnitude of U L_3-edge EXAFS spectrum after Fourier transformation for the biotic sample overlaid by the HUP standard. Spectra shown were collected in transmission mode.

HUP is the only significant solid phase to form in both the abiotic controls and the biotic experiments. Fittings of the EXAFS spectra (Fig. EA3) to the theoretical model indicates that the structure of the precipitate in all of the abiotic controls, as well as in all biotic experiments, is consistent with the mineral structure of HUP. Furthermore, and perhaps most importantly, the XAS results strongly suggest that, as predicted by surface precipitation theory, uranyl adsorption onto cell wall functional groups represents the first step in cell wall nucleation of uranyl phosphate minerals. Under the lower saturation state conditions studied, even though uranyl phosphate precipitation occurred in the system, uranium is present in the sample dominantly as adsorbed uranyl species. With increasing saturation state conditions, the adsorbed uranyl signal becomes overwhelmed with the uranyl phosphate precipitate, and under

the highest saturation states studied, the precipitation becomes clearly nucleated within the cell wall.

3.1.4. ICP-OES

In our discussion of the aqueous chemistry results, we refer to example saturation state conditions that correspond to the numbers in Fig. 7A and B. Both the starting and final concentrations for those example experiments are shown with corresponding number labels and arrows. Saturation state condition 1 represents the lowest saturation state studied; increasing saturation state condition numbers indicate increasing saturation state conditions. For saturation state conditions 2 and 3 (Fig. 7A), the abiotic controls removed significantly more U from solution than the *B. subtilis* biotic experiments performed at 0.62 g wet biomass/L. At saturation state condition 1, the biotic experiments removed slightly more U from solution than the abiotic controls. This slight increase in removed U is likely in part a result of U adsorption onto the biomass in the experiment, a result consistent with the XAS findings

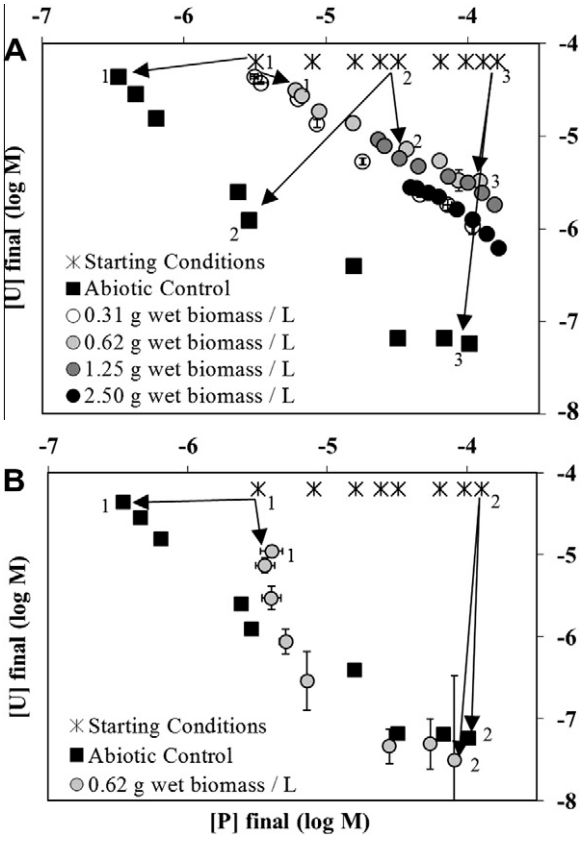

Fig. 7. Changes in the aqueous concentrations of U and P in the U experiments. (A) *B. subtilis*; (B) *S. oneidensis*. All experiments were performed in triplicate (symbols represent the mean). Error bars represent one standard deviation (note that some error bars are smaller than the symbol). Each arrow connects the starting condition (arrow tail, asterisks) to the final U and P concentrations in the abiotic control or biotic experiments (arrow head, squares and circles). The numerals "1", "2", and "3" represent saturation state conditions discussed in detail in the text and are presented here for reference.

for these low saturation state conditions. Additionally, the biotic experiments show an increase in final P concentrations relative to the experimental starting conditions at saturation state condition 1. This increase is likely due to P exuded from the bacteria during the experiment, and some of the enhanced U removal relative to the abiotic controls may be due to enhanced HUP precipitation from this additional P in the system. At saturation state conditions 2 and 3, the amount of P exuded represents a lower percentage of the total P in the experimental systems, and no significant increase in P is observed in those systems. Under all saturation states investigated, the abiotic controls removed more P from solution than did the biotic experiments relative to the starting conditions.

As the bacterial concentration was varied from 0.31 to 2.50 g (wet mass)/L, the amount of U removed from solution did not exhibit a consistent trend as a function of bacterial concentration (Fig. 7A). At all of the bacterial concentrations studied, the abiotic controls removed more U from solution at saturation state conditions 2 and 3 than did the biotic experiments. With increasing bacterial concentration, the final aqueous P concentration in the biotic experiments increased as well, likely due to bacterial exudates which contain P. However, the relative increase in P concentration decreased as the saturation state increased to condition 3.

Shewanella oneidensis biotic experiments removed slightly more U from solution at low saturation states (condition 1) than did the abiotic controls, but the two types of experiments removed approximately equal concentrations of U from solution under higher saturate state conditions (Fig. 7B, condition 2). The abiotic controls removed up to one log unit more P from solution at low saturation states than did the biotic experiments. Similar to the *B. subtilis* biotic experiments, the lowest saturation state *S. oneidensis* biotic experiments exhibited elevated final P concentrations, relative to both the starting conditions and the abiotic controls. This elevated P concentration is likely due to P that is exuded from the bacteria. The bacterially-exuded P in the *S. oneidensis* system is more readily available for U removal than the P exuded by *B. subtilis*, as evidenced by the greater removal of U from solution at the lowest saturation state condition in the *S. oneidensis* system relative to the *B. subtilis* system (Fig. 7B and A, respectively). At high saturation states, there was no significant difference in final U and P concentrations between the abiotic controls and the biotic experiments in the *S. oneidensis* system.

The higher aqueous U concentrations in the biotic experiments relative to the abiotic controls are not likely caused by nucleation kinetics effects. If the presence of the bacteria accelerated the nucleation kinetics, a result consistent with the presence of the smaller crystals in the biotic experiments relative to the abiotic controls, then one would expect lower concentrations of U to remain in solution as faster precipitation kinetics usually cause more complete precipitation reactions (Kasama and Murakami, 2001; Fritz and Noguera, 2009). Similarly, cell wall adsorption of U should cause enhanced removal of U from solution relative to the abiotic control experiments (Fowle

et al., 2000; Gorman-Lewis et al., 2005; Knox et al. 2008). However, the opposite occurs in most of our experiments, with higher aqueous U concentrations in the *B. subtilis* biotic experiments. The concentration of bacteria in the system does not significantly affect the extent of U and P removal within a range of 0.31–2.50 g wet biomass/L (Fig. 7A), also suggesting that U adsorption onto the bacteria does not control U concentrations in the higher saturation state experiments. This behavior is not a result of increased saturation state conditions in biotic experiments, since higher saturation states would result in less U remaining in solution in the biotic experiments compared to the abiotic controls (Ohnuki et al., 2005).

Elevated U concentrations can be caused by inhibition of precipitation by aqueous U complexation with organic exudates. To test whether aqueous U–organic complexes affected the extent of precipitation and were the cause for the observed elevated aqueous U concentrations in the biotic experiments, we used an organic exudate solution to perform a cell-free control experiment. Fig. 8 shows that at low saturation states (condition 1), the exudate solution contained an elevated P concentration relative to both the starting conditions and the abiotic control, confirming that bacteria exude P into solution. This effect is less apparent as the experimental P concentration increases. At the lowest saturation states investigated, there was no significant removal of U by the exudate solution, which is consistent with the XAS results which show that at low saturation states, U is dominantly removed by adsorption to cell walls. This also suggests that the exuded P is present as an organo-phosphate and is unavailable for precipitation with U. If the exudates contained orthophosphate, we would expect to observe enhanced U removal in the exudates solutions relative to the abiotic controls. As the saturation state increases to conditions 2 and 3, the exudate solution removes more U from solution than the biotic experiments, but removes less U from solution than the abiotic controls. These results suggest that U–organic aqueous complexes form under the experimental conditions, accounting for at least a portion of the increased final U concentration in the biotic experiments. However, because the exudate solution experiments result in more U removal than do the biotic experiments, it is evident that these aqueous complexes only account for a portion of the elevated U concentrations in the biotic experiments, and that another process also contributes to the observed elevated U concentrations in the biotic experiments.

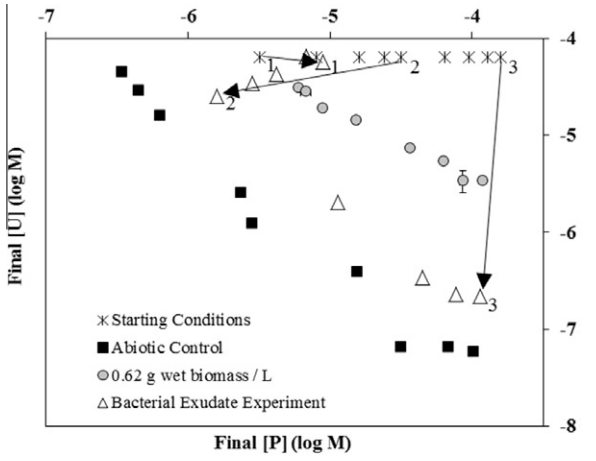

Fig. 8. Aqueous chemistry results for the bacterial exudate experiment (shown as hollow triangles) compared to aqueous chemistry results for the U system (as shown in Fig. 7A). Each arrow connects the starting condition (arrow tail, asterisks) to the final U and P concentrations in the abiotic control or biotic experiments (arrow head, squares and circles). The numerals "1", "2", and "3" represent saturation state conditions discussed in detail in the text and are presented here for reference.

3.1.5. Solubility

Complexation of U with organic exudates explains at least part of the enhanced U concentrations observed in the biotic experiments; however, at higher initial P concentrations, complexation does not explain the discrepancy between the abiotic controls and the biotic experiments. It is under these conditions that we observed cell wall mineralization and smaller particle sizes. These particles appear to be plate-like in morphology, with edge dimensions of much less than 30 nm in all dimensions. It is possible that the solubility of these nanoparticles is higher than the solubility of the much larger abiotic precipitates, and our solubility experiments were designed to test this hypothesis.

Fig. 9 depicts the experimental measurements of the solubility of the isolated biogenic precipitates (isolated from biotic U10). The measured U and P concentrations attained steady-state values by the time the first sample was extracted from the experiments, and maintained the steady-state for the duration of the experiment. The average steady-state log molalities of total U and P in solution were -4.34 ± 0.07 and -3.13 ± 0.08, respectively, with no consistent change in concentration after 2 days. The solubility product of HUP, determined by Gorman-Lewis et al. (2009) using 300 μm crystals, was used to calculate an expected solubility of macroscopic HUP crystals for comparison. For these calculations, we account for aqueous U and P speciation using the reactions and equi-

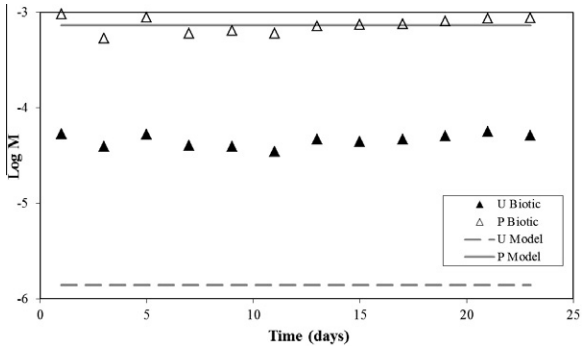

Fig. 9. Measured U and P concentrations from the solubility experiments involving biogenic hydrogen uranyl phosphate (HUP) precipitates. Model P concentrations were fixed at the average experimental value, and the model U line is the calculated U concentration in equilibrium with macroscopic HUP, using the *Ksp* value reported by Gorman-Lewis et al. (2009).

librium constants shown in Table EA1. At the measured equilibrium P concentration of our biogenic HUP solubility experiment, macroscopic HUP would be in equilibrium with a solution with a U log molality of −5.86 (−0.10/+0.08). The biogenic HUP exhibited a U concentration approximately 1.5 orders of magnitude higher than the concentration calculated for macroscopic HUP, suggesting that the particle size of these nanoscale-sized particles can exert a large influence on their solubilities. The results of the solubility measurements suggest that in addition to the effect of the aqueous U-exudate complexation, the size of the biogenic nanoprecipitates that form under high saturation state conditions likely contributes to the enhanced U concentrations that we observed in the biotic experiments.

3.1.6. Effects of bacteria on uranyl phosphate precipitation

Our results present evidence for passive cell wall biomineralization, a type of biomineralization in which the high binding affinity of cell walls for aqueous metal cations creates nucleation sites for mineral precipitation reactions in saturated systems. Although it is not clear from our data which cell wall functional groups are involved and what the exact precipitation mechanism is, the data demonstrate unequivocally that the presence of bacteria in some precipitating systems can alter the extent and morphology of the precipitation reaction, and is likely to affect the fate and mobility of the precipitating elements.

Passive cell wall biomineralization and the formation of nanoprecipitates of uranyl phosphate could significantly affect the mobility of U compared to the mobility exhibited if the precipitation occurred without bacteria present. Nanoprecipitates of uranyl phosphate may be released from the cell walls in which they formed after cell death, and due to their small size, the particles may be highly mobile in a geologic matrix. In addition, as our data suggest, nanoprecipitates can exhibit markedly higher solubilities than macro-scale crystals, and organic bacterial exudates can form aqueous complexes with dissolved uranium. Both of these processes affect the mobility of uranium in the aqueous phase, increasing the equilibrium concentration of U in solution at a given P concentration.

3.2. Lead system

3.2.1. TEM

Fig. 10 shows TEM micrographs of biotic samples under high and low saturation states (biotic Pb4 and Pb8). All of the electron dense (dark) particles in the bulk solution in the figure represent the mineral precipitate. The mineral precipitates in these images exhibit the same morphology and are similar in size (note that the scale bars are different in each micrograph). It is also evident that although the precipitate and the bacteria are in contact at some points, the contact appears to be coincidental only and no strong spatial correlation exists. We conclude from this visual evidence that passive cell wall mineralization does not occur in the Pb system under any of the saturation state conditions investigated.

3.2.2. XRD

The solid run products from biotic experiments Pb4, Pb6, and Pb8 were analyzed by XRD (Fig. EA4). The diffractograms for these samples exhibit the same peaks, suggesting that the precipitate in each biotic experiment was the same mineral, a result that is consistent with the TEM results above. Therefore, the precipitate in the Pb system is unaffected by varying saturation states within the range investigated in this study. Additionally, the diffractograms of the biotic experiments are all consistent with the reference pattern (ICDD 00-002-0750) for lead phosphate ($Pb_3(PO_4)_2$). XRD analyses were not performed on the abiotic controls due to the difficulty of harvesting a large enough mass of precipitate at the low Pb concentrations investigated.

3.2.3. ICP-OES

Under saturation state condition 1, the abiotic controls removed half a log unit less Pb from solution than did the biotic experiments (Fig. 11). Under this condition, the biotic experiments exhibited an increase in the final concentration of P relative to the abiotic controls and the starting condition. This increase in P in the biotic experiments, which is not seen in the abiotic controls, is likely a result of P exuded from the bacteria during the experiment.

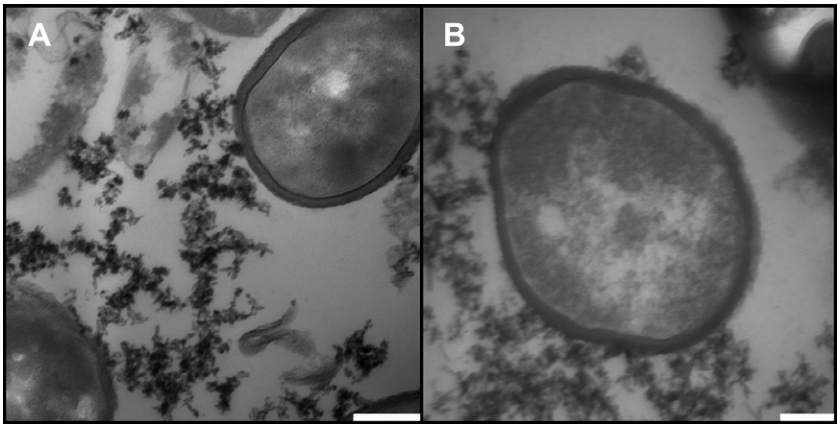

Fig. 10. TEM bright field images for Pb system: (A) Biotic Pb4 experiment (scale bar is 200 nm); (B) Biotic Pb8 (scale bar is 100 nm).

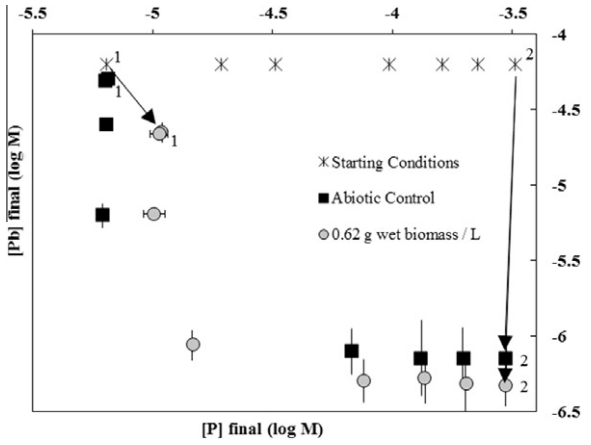

Fig. 11. Changes in the aqueous concentrations of Pb and P in the Pb experiments with *B. subtilis*. All experiments were performed in duplicate. Error bars represent one standard deviation (note that some error bars are smaller than the symbol). Each arrow connects the starting condition (arrow tail, asterisks) to the final Pb and P concentrations in the abiotic control or biotic experiments (arrow head, squares and circles). The numerals "1" and "2" represent saturation state conditions discussed in detail in the text and are presented here for reference.

Therefore, if the exuded P is at least in part present as orthophosphate, the enhanced Pb removal from solution in the biotic case could be due to enhanced $Pb_3(PO_4)_2$ precipitation due to the elevated saturation state that results from the exuded P. Alternatively, the enhanced removal in the biotic experiments could be due to Pb adsorption onto the biomass in the biotic experiments. At saturation state condition 2, the extents of Pb removal by the abiotic controls and the biotic experiments were not significantly different, nor did the P concentration change during the course of either the biotic or abiotic experiments.

3.2.4. Effect of bacteria on lead phosphate precipitation

The Pb system results demonstrate that the presence of bacteria does not strongly affect the extent or nature of Pb–phosphate precipitation under the conditions studied. Under low saturation state conditions, we observed enhanced removal of Pb from solution in the biotic systems relative to the abiotic controls, and this effect could be due either to the P that is exuded by the bacteria or to biomass adsorption of Pb. The bacteria do not affect the mineralogy nor the morphology of the precipitates in the Pb system, and consistent with these observations, our TEM images showed little or no association between the bacteria and the precipitate.

3.3. Calcium system

3.3.1. TEM

Under low saturation state conditions (Fig. 12A and B), the precipitates in both the abiotic controls (abiotic Ca7) and the biotic experiments (biotic Ca7) exhibit plate-like morphologies with average dimensions of approximately $50 \times 50 \times 10$ nm. Under higher saturation state conditions (Fig. 12C and D) the precipitate in the abiotic control (abiotic Ca11) exhibits the same characteristics as the abiotic control precipitate at low saturation states. However, the biotic experiment at high saturation states (biotic Ca11) produces smaller precipitates, with average dimensions of approximately $20 \times 20 \times <10$ nm. In Fig. 12B and D, there appears to be a spatial association between the mineral precipitate and the cell wall; however, it is uncertain whether this association is coincidental or a result of the cell wall involvement in the precipitation process. Therefore, although there is no evidence that passive cell wall nucleation occurs in this system under the investigated conditions, the presence of the bacteria affects the size of the mineral precipitate under high saturation state conditions.

3.3.2. XRD

Biotic Ca4 and abiotic and biotic Ca7 and Ca11 samples were characterized with XRD (Fig. 13). The abiotic controls each exhibit distinct peaks (e.g., at 2θ equal to 16.3, 26.1, 31.7, and 32.6), but the peaks in the biotic experiment diffractograms are less distinct, with significant peak broadening becoming more apparent with increasing saturation state. For example, in the diffractogram for biotic Ca11, the peaks at 2θ of 26.1, 31.7, and 32.6 appear to be one broad peak instead of the three distinct peaks seen in abiotic Ca11. The peak broadening effect that is evident at the high saturation states in the biotic experiments likely results from the formation of smaller precipitates under these conditions, as observed in the TEM images (Fig. 12D). Furthermore, the diffractograms from all of the Ca experiments are consistent with the reference diffractograms (ICDD 01-071-5049) for hydroxylapatite (HA, $Ca_{10}(PO_4)_6(OH)_2$), suggesting that HA is the dominant precipitate to form under all of the experimental conditions.

3.3.3. ICP-OES

Under virtually all of the saturation state conditions studied, the bacteria do not affect the extent of Ca removal during precipitation relative to the abiotic controls (Fig. 14). The bacteria do, however, release P into solution, resulting in higher final P concentrations in solution relative to both the abiotic controls and the starting conditions. With increasing experimental P concentration, the input of P from the bacteria becomes less important relative to the starting P concentration. At the highest saturation states studied (condition 2), the biotic samples exhibit Ca concentrations that are approximately 0.25 log molality units higher than those of the abiotic controls. As we observed in the U experiments, the elevated aqueous Ca concentrations remaining in solution in the biotic experiments are likely a result of aqueous Ca complexes with organic exudates. These complexes render the Ca unavailable for mineral precipitation, and as a result the remaining aqueous Ca concentrations in the biotic experiments are elevated relative to the abiotic controls.

3.3.4. Effect of bacteria on calcium phosphate precipitation

The results of the Ca experiments indicate that the presence of bacteria does not affect the extent of Ca precipitation from solution, except at the highest saturation state

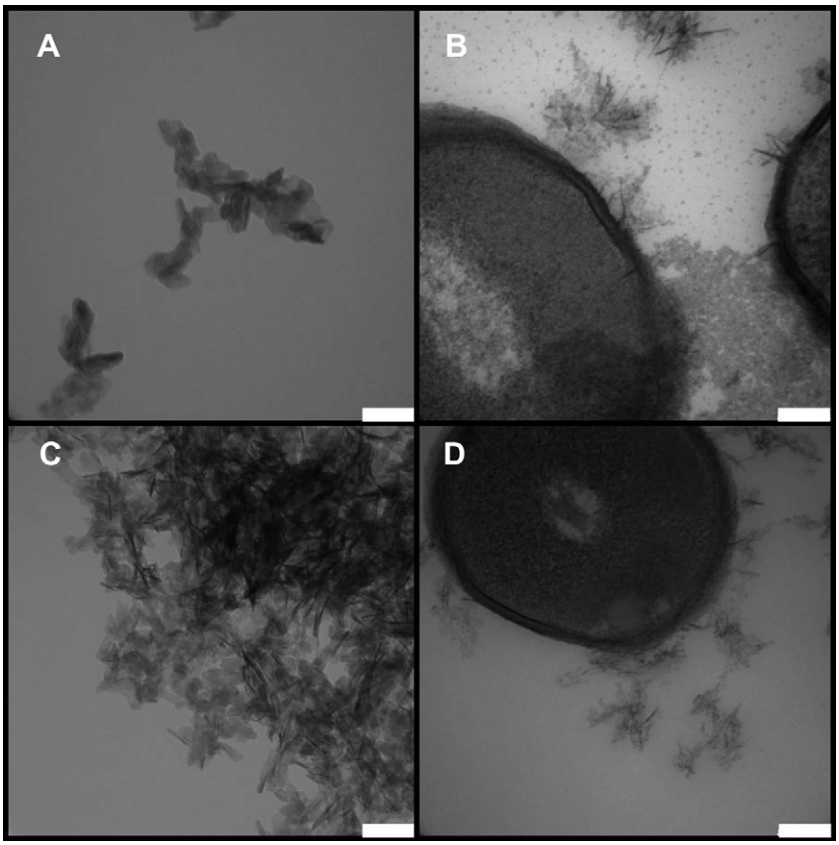

Fig. 12. TEM bright field images for Ca system: (A) Abiotic Ca7 control; (B) Biotic Ca7 experiment; (C) Abiotic Ca11 control; (D) Biotic Ca11 experiment. All scale bars are 100 nm.

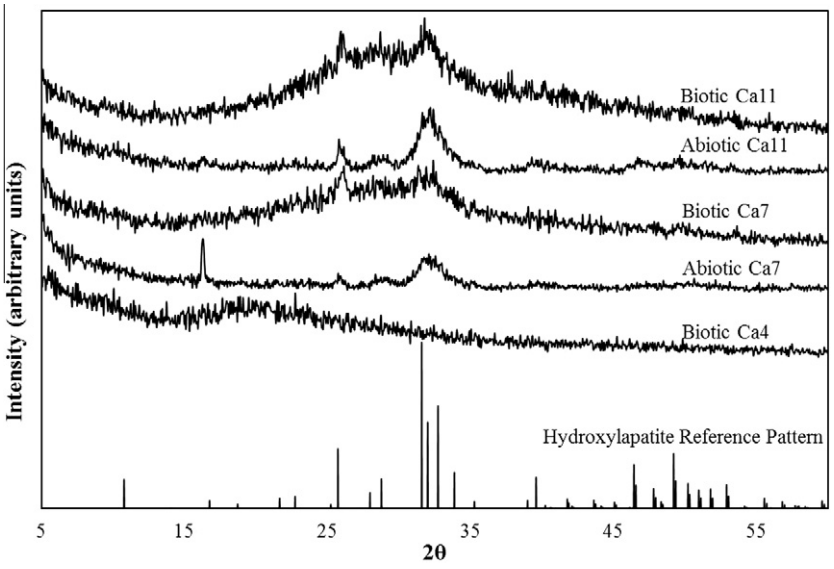

Fig. 13. XRD data from run-products of Ca experiments.

conditions investigated, where binding with bacterial exudates may affect the extent of Ca removal. Bacterial cells do not affect the mineralogy of the precipitates in the Ca system. However, the presence of bacteria results in a more fibrous morphology of the precipitates compared to that seen in the abiotic controls, and results in a decrease in the size of the precipitate under high saturation state conditions, as indicated by the TEM results. The size effect of the

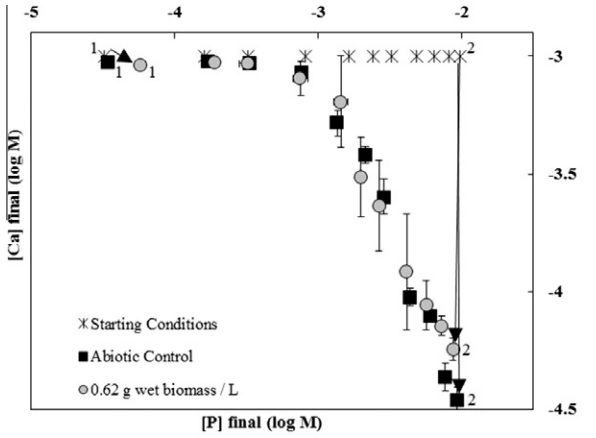

Fig. 14. Changes in the aqueous concentrations of Ca and P in the Ca experiments with *B. subtilis*. All experiments were performed in duplicate. Error bars represent one standard deviation (note that some error bars are smaller than the symbol). Each arrow connects the starting condition (arrow tail, asterisks) to the final Ca and P concentrations in the abiotic control or biotic experiments (arrow head, squares and circles). The numerals "1" and "2" represent saturation state conditions discussed in detail in the text and are presented here for reference.

bacteria in the Ca experiments is likely due to the presence of organic bacterial exudates in solution and the interaction of these molecules with the precipitating HA particles. Lebron and Suarez (1996) reported a similar effect on the size of calcite precipitates in the presence of varying concentrations of dissolved organic carbon (DOC). With increased concentrations of DOC, Lebron and Suarez (1996) observed a decrease in calcite particle sizes from >100 μm at a DOC concentration of 0.02 mM to <2 μm at a DOC concentration of 0.15 mM. Consistent with this observation, the biotic experiment diffractograms exhibited a general peak broadening effect, which became more pronounced with increasing saturation states. Studies have reported that particle size and peak width in XRD diffractograms are inversely correlated, such that smaller particles produce wider peaks in the diffractogram relative to the same mineral with a larger particle size (Weibel et al., 2005; Sanchez-Bajo et al., 2006). The observed gradual peak broadening effect in the biotic experiments with increasing saturation state suggests that the precipitate size and/or crystallinity decrease as the saturation state increases.

4. CONCLUSIONS

In this study, we investigated the effects of non-metabolizing bacteria on the precipitation of metal phosphates under a range of saturation states. Our results demonstrate several distinct bacterial effects. At high saturation states in the U system, we observed passive cell wall nucleation of uranyl phosphate minerals within the cell wall framework of both *B. subtilis* and *S. oneidensis* cells. These nucleated particles, although of the same mineralogy and morphology as forms under abiotic conditions, were dramatically smaller than the abiotic precipitates. Furthermore, the extent of U removal in the biotic systems was significantly reduced relative to the abiotic controls, in part due to the elevated solubility of the smaller nucleated particles, and in part due to the presence of bacterial exudate molecules that formed aqueous complexes with U and prevented the same degree of uranyl phosphate precipitation as occurred in the abiotic experiments. We did not observe the same passive cell wall mineralization phenomenon in the Ca or Pb systems. However, the presence of bacteria did decrease the size of the precipitates in the Ca system at high saturation state. Our experimental results strongly suggest that the bacterial effects that we observed are likely to be element and/or saturation state specific. It is likely that highly stable metal-phosphoryl binding, such as exists in the U system, is required to trigger metal–phosphate cell wall mineralization.

Our observations provide the first comprehensive evidence for the passive cell wall biomineralization of metal phosphates, in which the high binding affinity of cell walls for aqueous metal cations creates nucleation sites for mineral precipitation reactions in saturated systems. These nucleation sites likely promote heterogeneous nucleation of metal phosphates on or in the cell wall through surface complexation reactions, as seen by Fowle and Fein (2001). The passive cell wall biomineralization mechanism does not change the mineral that precipitates. It does, however, exert a strong control on the size of the precipitate that forms during the experiments.

ACKNOWLEDGMENTS

Funding for this research was provided in part by a U.S. Department of Energy, Office of Science and Technology and International (OST&I) grant under the Source Term Thrust program, and in part by a U.S. Department of Energy, Environmental Remediation Science Program grant. The experiments and analyses were performed at the Center for Environmental Science & Technology, University of Notre Dame. The XAS measurements were obtained at the MRCAT-10-ID Beamline at the Advanced Photon Source (APS), Argonne National Laboratory. TEM images were obtained at the Integrated Imaging Facility at the University of Notre Dame and at the Institut de Minéralogie et de Physique des Milieux Condensés, Paris, France. We thank Andrew Quicksall for providing suggestions and feedback throughout the project. Three journal reviews were extremely helpful, and significantly improved the presentation of this work.

APPENDIX A. SUPPLEMENTARY DATA

Supplementary data associated with this article can be found, in the online version, at doi:10.1016/j.gca.2011.02.030.

REFERENCES

Ams D. A., Fein J. B., Dong H. L. and Maurice P. A. (2004) Experimental measurements of the adsorption of *Bacillus subtilis* and *Pseudomonas mendocina* onto Fe-oxyhydroxide-coated and uncoated quartz grains. *Geomicrobiol. J.* **21**, 511–519.

Archibald D. D., Qadri S. B. and Gaber B. P. (1996) Modified calcite deposition due to ultrathin organic films on silicon substrates. *Langmuir* **12**, 538–546.

Arp G., Hofmann J. and Reitner J. (1998) Microbial fabric formation in spring mounds ("Microbialites") of Alkaline Salt Lakes in the Badain Jaran Sand Sea, PR China. *Palaios* **13**, 581–592.

Bazylinski D. A. and Moskowitz B. M. (1997) Microbial biomineralization of magnetic iron minerals: microbiology, magnetism and environmental significance. In *Geomicrobiology: Interactions between Microbes and Minerals* (eds. J. F. Banfield and K. H. Nealson). Mineralogical Society of America, Washington DC, pp. 181–223.

Beazley M. J., Martinez R. J., Sobecky P. A., Webb S. M. and Taillefert M. (2007) Uranium biomineralization as a result of bacterial phosphatase activity: insights from bacterial isolates from a contaminated subsurface. *Environ. Sci. Technol.* **41**, 5701–5707.

Ben Chekroun K., Rodriguez-Navarro C., Gonzalez-Munoz M. T., Arias J. M., Cultrone G. and Rodriguez-Gallego M. (2004) Precipitation and growth morphology of calcium carbonate induced by *Myxococcus xanthus*: implications for recognition of bacterial carbonates. *J. Sed. Res.* **74**, 868–876.

Beveridge T. J. and Murray R. G. E. (1976) Uptake and retention of metals by cell walls of *Bacillus subtilis*. *J. Bacteriol.* **127**, 1502–1518.

Bonny S. and Jones B. (2003) Microbes and mineral precipitation, Miette Hot Springs, Jasper National Park, Alberta, Canada. *Can. J. Earth Sci.* **40**, 1483–1500.

Borrok D., Aumend K. and Fein J. B. (2007) Significance of ternary bacteria–metal–natural organic matter complexes determined through experimentation and chemical equilibrium modeling. *Chem. Geol.* **238**, 44–62.

Bosak T. and Newman D. K. (2005) Microbial kinetic controls on calcite morphology in supersaturated solutions. *J. Sed. Res.* **75**, 190–199.

Boyanov M. I., O'Loughlin E. J., Roden E. E., Fein J. B. and Kemner K. M. (2007) Adsorption of Fe(II) and U(VI) to carboxyl-functionalized microspheres: the influence of speciation on uranyl reduction studied by titration and XAFS. *Geochim. Cosmochim. Acta* **71**, 1898–1912.

Braissant O., Cailleau G., Dupraz C. and Verrecchia E. P. (2003) Bacterially induced mineralization of calcium carbonate in terrestrial environments: the role of exopolysaccharides and amino acids. *J. Sed. Res.* **73**, 485–490.

Bunker G. (2010) *Introduction to XAFS: A Practical Guide to X-ray Absorption Fine Structure Spectroscopy*, 1st ed. Cambridge University Press, New York.

Châtellier X., Fortin D., West M. M., Leppard G. G. and Ferris F. G. (2001) Effect of the presence of bacterial surfaces during the synthesis of Fe oxides by oxidation of ferrous ions. *Eur. J. Mineral.* **13**, 705–714.

Châtellier X., West M. M., Rose J., Fortin D., Leppard G. G. and Ferris F. G. (2004) Characterization of iron-oxides formed by oxidation of ferrous ions in the presence of various bacterial species and inorganic ligands. *Geomicrobiol. J.* **21**, 99–112.

Dekov V. M., Petersen S., Garbe-Schönberg C.-D., Kamenov G. D., Perner M., Kuzmann E. and Schmidt M. (2010) Fe–Si–oxyhydroxide deposits at a slow-spreading centre with thickened oceanic crust: the Lilliput hydrothermal field (9°33′S, Mid-Atlantic Ridge). *Chem. Geol.* **278**, 186–200.

Demergasso C. S., Chong G., Escudero L., Mur J. J. P. and Pedros-Alio C. (2007) Microbial precipitation of arsenic sulfides in Andean salt flats. *Geomicrobiol. J.* **24**, 111–123.

Deo R. P., Songkasiri W., Rittmann B. E. and Reed D. T. (2010) Surface complexation of neptunium(V) onto whole cells and cell components of *Shewanella alga*: modeling and experimental study. *Environ. Sci. Technol.* **44**, 4930–4935.

Douglas S. and Beveridge T. J. (1998) Mineral formation by bacteria in natural microbial communities. *FEMS Microbiol. Ecol.* **26**, 79–88.

Dupraz C., Reid R. P., Braissant O., Decho A. W., Norman R. S. and Visscher P. T. (2009) Processes of carbonate precipitation in modern microbiol mats. *Earth Sci. Rev.* **96**, 141–162.

Farley K. J., Dzombak D. A. and Fmm M. (1985) A surface precipitation model for the sorption of cations on metal-oxides. *J. Colloid Interf. Sci.* **106**, 226–242.

Fein J. B., Daughney C. J., Yee N. and Davis T. A. (1997) A chemical equilibrium model for metal adsorption onto bacterial surfaces. *Geochim. Cosmochim. Acta* **61**, 3319–3328.

Ferris F. G., Fyfe W. S. and Beveridge T. J. (1987) Bacteria as nucleation sites for authigenic minerals in a metal-contaminated lake sediment. *Chem. Geol.* **63**, 225–232.

Fortin D. and Langley S. (2005) Formation and occurrence of biogenic iron-rich minerals. *Earth Sci. Rev.* **72**, 1–19.

Fowle D. A., Fein J. B. and Martin A. M. (2000) Experimental study of uranyl adsorption onto *Bacillus subtilis*. *Environ. Sci. Technol.* **34**, 3737–3741.

Fowle D. A. and Fein J. B. (2001) Quantifying the effects of *Bacillus subtilis* cell walls on the precipitation of copper hydroxide from aqueous solution. *Geomicrobiol J.* **18**, 77–91.

Fritz B. and Noguera C. (2009) Mineral Precipitation Kinetics. *Rev. Mineral. Geochem.* **70**, 371–410.

Fuller C. C., Bargar J. R. and Davis J. A. (2003) Molecular-scale characterization of uranium sorption by bone apatite materials for a permeable reactive barrier demonstration. *Environ. Sci. Technol.* **37**, 4642–4649.

Gorman-Lewis D., Elias P. E. and Fein J. B. (2005) Adsorption of aqueous uranyl complexes onto *Bacillus subtilis* cells. *Environ. Sci. Technol.* **39**, 4906–4912.

Gorman-Lewis D., Shvareva T., Kubatko K. A., Burns P. C., Wellman D. M., McNamara B., Syzmanowski J. E. S., Navrotsky A. and Fein J. B. (2009) Thermodynamic properties of autunite, uranyl hydrogen phosphate, and uranyl orthophosphate from solubility and calorimetric measurements. *Environ. Sci. Technol.* **43**, 7416–7422.

Hammes F., Boon N., de Villiers J., Verstraete W. and Siciliano S. D. (2003) Strain-specific ureolytic microbial calcium carbonate precipitation. *Appl. Environ. Microbiol.* **69**, 4901–4909.

Helgeson H. C., Kirkham D. H. and Flowers G. C. (1981) Theoretical prediction of the thermodynamic behavior of aqueous-electrolytes at high pressures and temperatures. 4. Calculation of activity-coefficients, osmotic coefficients, and apparent molal and standard and relative partial molal properties to 600-degrees-C and 5 kb. *Am. J. Sci.* **281**, 1249–1516.

Hennig C., Panak P. J., Reich T., Rossberg A., Raff J., Selenska-Pobell S., Matz W., Bucher J. J., Bernhard G. and Nitsche H. (2001) EXAFS investigation of uranium(VI) complexes formed at *Bacillus cereus* and *Bacillus sphaericus* surfaces. *Radiochim. Acta* **89**, 625–631.

James R. E. and Ferris F. G. (2004) Evidence for microbial-mediated iron oxidation at the neutrophilic groundwater spring. *Chem. Geol.* **212**, 301–311.

Kasama T. and Murakami T. (2001) The effect of microorganisms on Fe precipitation rates at neutral pH. *Chem. Geol.* **180**, 117–128.

Kelly S. D., Kemner K. M., Fein J. B., Fowle D. A., Boyanov M. I., Bunker B. A. and Yee N. (2002) X-ray absorption fine structure determination of pH-dependent U-bacterial cell wall interactions. *Geochim. Cosmochim. Acta* **66**, 3855–3871.

Kirpichtchikova T. A., Manceau A., Spadini L., Panfili F., Marcus M. A. and Jacquet T. (2006) Speciation and solubility of heavy metals in contaminated soil using X-ray microfluorescence,

EXAFS spectroscopy, chemical extraction, and thermodynamic modeling. *Geochim. Cosmochim. Acta* **70**, 2163–2190.

Knox A. S., Brimon R. L., Kaplan D. I. and Paller M. H. (2008) Interactions among phosphate amendments, microbes and uranium mobility in contaminated sediments. *Sci. Total Environ.* **395**, 63–71.

Konhauser K. O., Fyfe W. S., Ferris F. G. and Beveridge T. J. (1993) Metal sorption and mineral precipitation by bacteria in 2 Amazonian river systems – Rio-Solimoes and Rio-Negro, Brazil. *Geology* **21**, 1103–1106.

Konhauser K. O. (1997) Bacterial iron biomineralization in nature. *FEMS Microbiol. Rev.* **20**, 315–326.

Konhauser K. O. (1998) Diversity of bacterial iron mineralization. *Earth Sci. Rev.* **43**, 91–121.

Kulczycki E., Ferris F. G. and Fortin D. (2002) Impact of cell wall structure on the behavior of bacterial cells as sorbents of cadmium and lead. *Geomicrobiol J.* **19**, 553–565.

Labrenz M., Druschel G. K., Thomsen-Ebert T., Gilbert B., Welch S. A., Kemner K. M., Logan G. A., Summons R. E., De Stasio G., Bond P. L., Lai B., Kelly S. D. and Banfield J. F. (2000) Formation of sphalerite (ZnS) deposits in natural biofilms of sulfate-reducing bacteria. *Science* **290**, 1744–1747.

Larese-Casanova P., Haderlein S. B. and Kappler A. (2010) Biomineralization of lepidocrocite and goethite by nitrate-reducing Fe(II)-oxidizing bacteria: effect of pH, bicarbonate, phosphate, and humic acids. *Geochim. Cosmochim. Acta* **74**, 3721–3734.

Lebron I. and Suarez D. L. (1996) Calcite nucleation and precipitation kinetics as affected by dissolved organic matter at 25 °C and pH >7.5. *Geochim. Cosmochim. Acta* **60**, 2765–2776.

Lefevre C. T., Bernadac A., Yu-Zhang K., Pradel N. and Wu L. F. (2009) Isolation and characterization of a magnetotactic bacterial culture from the Mediterranean Sea. *Environ. Microbiol.* **11**, 1646–1657.

Li W. C. and Wong M. H. (2010) Effects of bacteria on metal bioavailability, speciation, and mobility in different metal mine soils: a column study. *J. Soils Sediments* **10**, 313–325.

Lowentam H. A. (1981) Minerals formed by organisms. *Science* **211**, 1126–1131.

Lowenstam H. A. and Weiner S. (1989) *On Biomineralization*. Oxford University Press, New York.

Macaskie L. E., Bonthrone K. M., Yong P., and Goddard D. T. (2000) Enzymically mediated bioprecipitation of uranium by a Citrobacter sp.: a concerted role for exocellular lipopolysaccharide and associated phosphatase in biomineral formation. *Microbiology – UK* **146,** 1855-18.

Manceau A., Kersten M., Marcus M. A., Geoffroy N. and Granina L. (2007) Ba and Ni speciation in a nodule of binary Mn oxide phase composition from Lake Baikal. *Geochim. Cosmochim. Acta* **71**, 1967–1981.

Mann S., Didymus J. M., Sanderson N. P., Heywood B. R. and Aso Samper E. J. (1990) Morphological influence of functionalized and non-functionalized α, ω-dicarboxylates on calcite crystallization. *Journal of the Chemical Society – Faraday Transactions* **86**, 1873–1880.

Martell A. E. and Smith R. M. (2001) *NIST Critically selected stability constants of metal complexes, Version 6.0*. NIST Standard Reference Database 46. National Institute of Standards and Technology. Gaithersburg, MD.

Martinez R. J., Beazley M. J., Taillefert M., Arakaki A. K., Skolnick J. and Sobecky P. A. (2007) Aerobic uranium (VI) bioprecipitation by metal-resistant bacteria isolated from radionuclide- and metal-contaminated subsurface soils. *Environ. Microbiol.* **9**, 3122–3133.

McGrath K. M. (2001) Probing material formation in the presence of organic and biological molecules. *Adv. Mater.* **13**, 989–992.

Meldrum F. C. and Hyde S. T. (2001) Morphological influence of magnesium and organic additives on the precipitation of calcite. *J. Cryst. Growth* **231**, 544–558.

Morosin B. (1978) Hydrogen uranyl phosphate tetrahydrate, A hydrogen-ion solid electrolyte. *Acta Crystallogr. Sect. B: Struct. Sci.* **34**, 3732–3734.

Ndiba P., Axe L. and Boonfueng T. (2008) Heavy metal immobilization through phosphate and thermal treatment of dredged sediments. *Environ. Sci. Technol.* **42**, 920–926.

Newville M. (2001) IFEFFIT: interactive XAFS analysis and FEFF fitting. *J Synchrotron Radiat.* **8**, 322–324.

Newville M., Livins P., Yacoby Y., Rehr J. J. and Stern E. A. (1993) An improved background removal method for XAFS. In *Japanese Journal of Applied Physics Part 1 – Regular Papers, Short Notes & Review Papers*, vol. 32. Japan J Applied Physics, Japan. pp. 125–127.

Ohnuki T., Ozaki T., Yoshida T., Sakamoto F., Kozai N., Wakai E., Francis A. J. and Iefuji H. (2005) Mechanisms of uranium mineralization by the yeast *Saccharomyces cerevisiae*. *Geochim. Cosmochim. Acta* **69**, 5307–5316.

Perez-Gonzalez T., Jimenez-Lopez C., Neal A. L., Rull-Perez F., Rodriguez-Navarro A., Fernandez-Vivas A. and Iañez-Pareja E. (2010) Magnetite biomineralization induced by *Shewanella oneidensis*. *Geochim. Cosmochim. Acta* **74**, 967–979.

Ravel B. and Newville M. (2005) ATHENA, ARTEMIS, HEPHAESTUS: data analysis for X-ray absorption spectroscopy using IFEFFIT. *J. Synchrotron Radiat.* **12**, 537–541.

Ravel B., Grenier S., Renevier H. and Eom C. B. (2001) Valence selective DAFS measurements of Mn in La1/3Ca2/3MnO_3. *J. Synchrotron Radiat.* **8**, 384–386.

Rivadeneyra M. A., Martin-Algarra A., Sanchez-Navas A. and Martin-Ramos D. (2006) Carbonate and phosphate precipitation by *Chromohalobacter marismortui*. *Geomicrobiol. J.* **23**, 89–101.

Sanchez-Bajo F., Ortiz A. L. and Cumbrera F. L. (2006) Novel analytical model for the determination of grain size distributions in nanocrystalline materials with low lattice microstrains by X-ray diffractometry. *Acta Mater.* **54**, 1–10.

Schultze-Lam S., Fortin D., Davis B. S. and Beveridge T. J. (1996) Mineralization of bacterial surfaces. *Chem. Geol.* **132**, 171–181.

Schwertmann U., Cambier P. and Murad E. (1985) Properties of goethites of varying crystallinity. *Clay Clay Mineral.* **33**, 369–378.

Stern E. A., Newville M., Ravel B., Yacoby Y. and Haskel D. (1995) The UWXAFS Analysis Package – Philosophy and Details. In *Physica B*, vol. 208, pp. 117–120. Physica B. Elsevier Science, Amsterdam.

Sullivan L. A. and Koppi T. J. (1998) Iron staining of quartz beach sand in southeastern Australia. *J. Coastal Res.* **14**, 992–999.

Taylor K. G. and Boult S. (2007) The role of grain dissolution and diagenetic mineral precipitation in the cycling of metals and phosphorus: a study of a contaminated urban freshwater sediment. *Appl. Geochem.* **22**, 1344–1358.

Terzano R., Spagnuolo M., Medici L., Dorrine W., Janssens K. and Ruggiero P. (2007) Microscopic single particle characterization of zeolites synthesized in a soil polluted by copper or cadmium and treated with coal fly ash. *Appl. Clay Sci.* **35**, 128–138.

Tong H., Ma W., Wang L., Wan P., Hu J. and Cao L. (2004) Control over the crystal phase, shape, size and aggregation of calcium carbonate via a L-aspartic acid inducing process. *Biomaterials* **25**, 3923–3929.

Ulrich K. U., Singh A., Schofield E. J., Bargar J. R., Veeramani H., Sharp J. O., Bernier-Latmani R. and Giammar D. E. (2008)

Dissolution of biogenic and synthetic UO_2 under varied reducing conditions. *Environ. Sci. Technol.* **42**, 5600–5606.

Urrutia M. M. and Beveridge T. J. (1994) Formation of fine-grained silicate minerals and metal precipitates by a bacterial surface (*Bacillus subtilis*) and the implications in the global cycling of silicon. *Chem. Geol.* **116**, 261–280.

Warren L. A. and Ferris F. G. (1998) Continuum between sorption and precipitation of Fe(III) on microbial surfaces. *Environ. Sci. Technol.* **32**, 2331–2337.

Warren L. A., Maurice P. A., Parmar N. and Ferris F. G. (2001) Microbially mediated calcium carbonate precipitation: Implications for interpreting calcite precipitation and for solid-phase capture of inorganic contaminants. *Geomicrobiol. J.* **18**, 93–115.

Weibel A., Bouchet R., Boulc'h F. and Knauth P. (2005) The big problem of small particles: a comparison of methods for determination of particle size in nanocrystalline anatase powders. *Chem. Mater.* **17**, 2378–2385.

Wellman D. M., Pierce E. M. and Valenta M. M. (2007) Efficacy of soluble sodium tripolyphosphate amendments for the in-situ immobilisation of uranium. *Environ. Chem.* **4**, 293–300.

Williams R. J. P. (1984) An introduction to biominerals and the role of organic molecules in their formation. *Philos. Trans. R. Soc. London, Ser. B* **304**, 411–424.

Yu-Zhang K., Zhu K. L., Xiao T. and Wu L. F. (2009) Magnetotactic bacteria – a natural architecture leading from structure to possible applications. *Archit. Multifunct. Mater.* **1188**, 175–186.

Zabinsky S. I., Rehr J. J., Ankudinov A., Albers R. C. and Eller M. J. (1995) Multiple-scattering calculations of X-ray absortpion spectra. *Phys. Rev. B* **52**, 2995–3009.

Zhu Y., Zhang X., Chen Y., Xie Q., Lan J., Qian M. and He N. (2009) A comparative study on the dissolution and solubility of hydroxylapatite and fluorapatite at 25 °C and 45 °C. *Chem. Geol.* **268**, 89–96.

Associate editor: Karen Johannesson